

Department of Mechanical Engineering
FACULTY OF ENGINEERING AND DESIGN

FINAL YEAR BEng PROJECT REPORT (ME30227)

Experimental Assessment of an Optimass 6400 Mass Flow Meter for Determining CO₂ Vapour Quality

Tym Pakulski

05/05/2015



"I certify that I have read and understood the entry in the Student Handbook for the Department of Mechanical Engineering on Cheating and Plagiarism and that all material in this assignment is my own work, except where I have indicated with appropriate references. I agree that, in line with Regulation 15.3(e), if requested I will submit an electronic copy of this work for submission to a Plagiarism Detection Service for quality assurance purposes."

Author's signature:

Supervisor: *Dr. Roger Ngwompo*

Assessor: *Dr. Martin Ansell*

Experimental Assessment of a Krohne Optimass 6400 Mass Flow
Meter for Determining CO₂ Vapour Quality
Final Year Project Report

Tymon Pakulski

Department of Mechanical Engineering, University of Bath

In Collaboration with CERN - The European Organization for Nuclear Research

Supervised by Dr. Roger Ngwompo

Assessed by Dr. Martin Ansell

May 3, 2015

Abstract

Acknowledgments

Thanks to Dr. Roger Ngwompo, my academic supervisor, and Dr. Martin Ansell, FYP coordinator, for making my continued collaboration with CERN possible. I'd also like to thank Nicola Spadavecchia, Bart Verlaat and Jerome Noel for their technical support. Finally, my thanks to Paola Tropea, my industrial supervisor, for her sharp questions and crucial guidance throughout my research.

Terms and Acronyms

CERN The European Organization for Nuclear Research

Nikhef National Institute for Subatomic Physics, Amsterdam, Netherlands

HEP High-Energy Physics

CMS Compact Muon Solenoid - a CERN experiment

LHC Large Hadron Collider

2PACL Two-phase accumulator control loop A planned shutdown of the LHC between February 2013 and April 2015 for maintenance and upgrade.

CFCs Chlorofluorocarbons

TIF Tracker Integration Facility

PH-DT CERN Physics Department, Detector Technologies Group

EGM Entrained Gas Management

DAQ Data Acquisition

SCADA sc

PWM Pulse Width Modulation

R744 Refrigerant Code for CO₂

Sub-cooling sub

Interaction Point point

.csv Comma-Seperated Value

C₆F₁₄ Perflourohexane, a common industrial refrigerant and electrical insulator.

Symbols

Symbol	Property	Default Unit
H	Enthalpy	J
X	Vapour Quality	%
T	Temperature	°C
\dot{m}	Mass Flow Rate	kgs ⁻¹
P	Pressure	bar abs
\dot{Q}	Heat Load	Watts
ϕ	Void Fraction	%
G	Mass Flux	kgs ⁻¹ m ⁻²
I	Current	Amperes
V	Voltage	Volts
p	Power	Watts
ρ	Density	kgm ⁻³
v	velocity	ms ⁻¹
VPV	Vapour Phase Velocity	ms ⁻¹

Contents

1	Introduction	1
1.1	CO ₂ Cooling at CERN	1
1.2	2-Phase Accumulator Controlled Loop	1
1.3	Vapour Quality and 2-Phase Density	3
1.4	The Krohne Optimass 6400	4
1.5	Aims, Objectives and Documentation	4
2	Literature Review	6
2.1	Behaviour of 2-Phase CO ₂	6
2.2	Determining Vapour Quality	8
2.3	2-Phase Performance of Coriolis Flow Meters	9
3	Methods	11
3.1	Experimental Methods	11
3.1.1	Apparatus	11
3.1.2	Control and Data Acquisition	12
3.1.3	Variables and Assumptions	15
3.1.4	Test Protocol	16
3.2	Data Analysis Methods	17
3.2.1	Export Pre-Processing	17
3.2.2	Data Processing and Visualisation	19
3.2.3	Calculation of Reference Conditions	19
3.3	Calculation of Vapour Surface Velocity	20
4	Results	21
4.1	Overview	21
4.2	Mass Flow Trend	23
4.3	Temperature Trend	26
5	Discussion	30
5.1	Overview	30
5.2	Mass Flow Rate Trend	30
5.3	Temperature Trend	31
5.4	Errors and Uncertainty	31
6	Conclusions	33
7	Future Work	34
A	The TIF Cooling System	38
B	Krohne Calibration and Sizing Documents	41
C	Dummy Load Heater Module Mechanical Design	43

D MATLAB Code

47

E Raw Data

48

1. Introduction

CERN's PH-DT group is undertaking extensive research and development in the area of evaporative CO₂ cooling for particle detectors. A crucial parameter in the design and commissioning of these systems is vapour quality - the mass fraction of fluid that is vapour. Krohne, a supplier of instrumentation for the process industry, has approached CERN with a new instrument with potential to indirectly determine vapour quality through a measurement of 2-phase density. This study seeks to evaluate this promising new technology that would be directly relevant to the coming decade of R&D.

1.1 CO₂ Cooling at CERN

The particle detectors at CERN's various experiments require cooling to manage the heat load of the detector electronics, radiation from the interaction point and heat leak from the ambient environment. Evaporative CO₂ cooling has become the predominant candidate technology for future particle trackers in HEP. CO₂'s combination of thermodynamic properties and radiation hardness make it ideal for HEP applications - it can be used in highly radioactive areas and is considered environmentally friendly. In addition, it cools efficiently in small-diameter tubes, minimising the material budget - a crucial metric representing the amount of non-instrumentation material inside the particle detector.

The C_6F_{14} current cooling system for the pixel detector, the innermost layer of the CMS tracker, is being replaced with a CO₂ system and a transition to this technology is foreseen for the entire CMS tracker by the end of 2024.

1.2 2-Phase Accumulator Controlled Loop

The CO₂ systems at CERN implement the 2PACL design. [?]. This involves pumping liquid coolant into the the detector, where it is expanded and cools its surroundings by partially evaporating. After cooling the detector with the latent heat of vaporisation, the mix of liquid and vapour returns to the plant by way of a condenser, which returns it to pure liquid phase for pumping. An accumulator filled with 2-phase fluid sits on

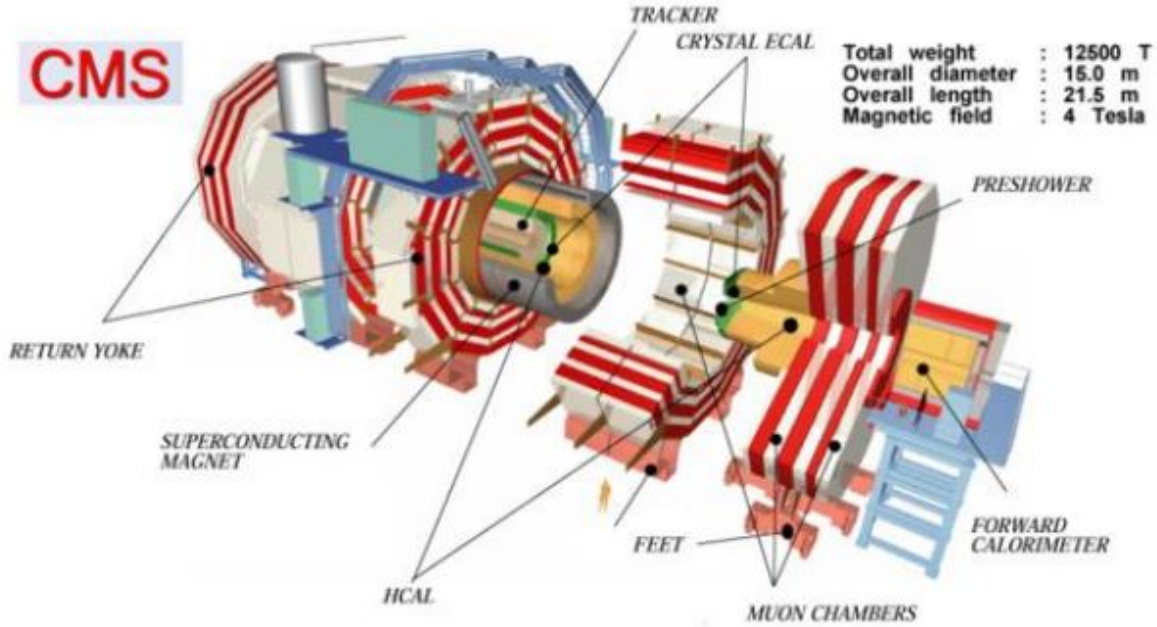


Figure 1.1: A diagram of the CMS particle detector on the LHC. [16]

the return line of the circuit, its pressure determining the position of the coolant temperature (and pressure as both are saturated), and therefore the position of the cooling cycle on the P-h diagram. Accumulator pressure is regulated using an array of heaters and a heat exchanger with an independent chiller circuit that also cools the condenser. The cycle and a schematic of the 2PACL concept are shown in figure 1.2.

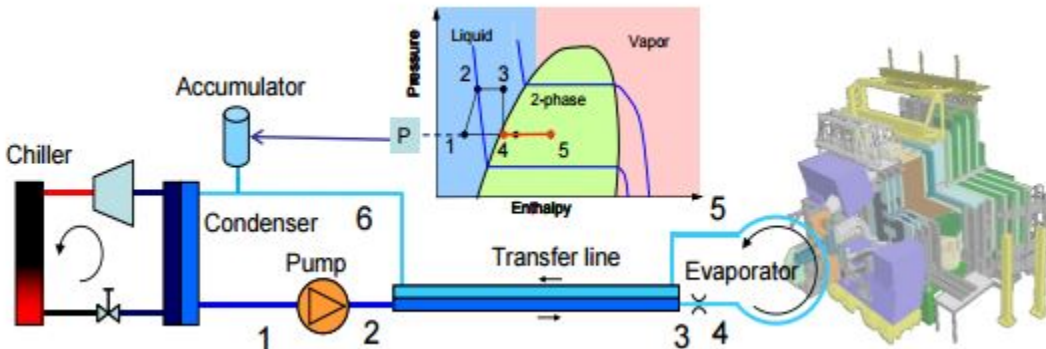


Figure 1.2: A schematic of the 2PACL concept as implemented in Thermal Control System of the LHCb Velo project at CERN [17]

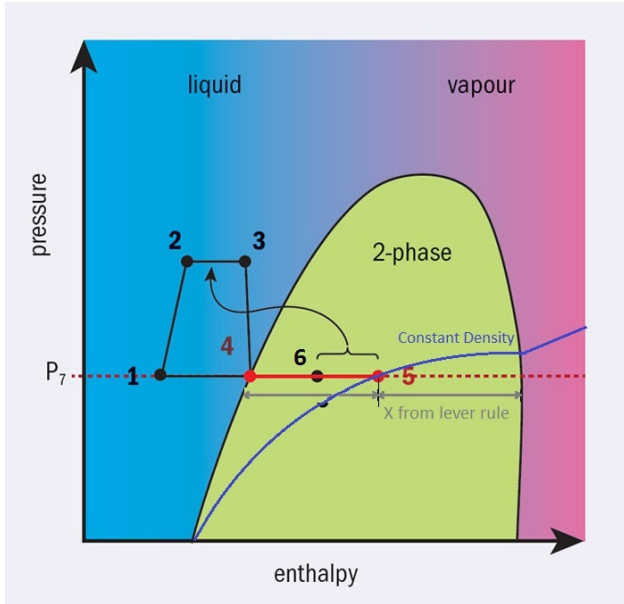


Figure 1.3: Principle for determining vapour quality, X , from two-phase density. Adapted from B. Verlaat. [22]

1.3 Vapour Quality and 2-Phase Density

Vapour quality refers to the fraction of a fluid's mass that is in the vapour phase.

$$X = \frac{m_{vapour}}{m_{fluid}} \quad (1.1)$$

In 2PACL cooling systems, the vapour quality after the coolant evaporates in the detector volume is an essential system parameter indicating the amount of evaporation that has occurred. The quality determines how far from the coolant is from dry-out, where a dramatic decrease in heat transfer coefficients may occur, causing a sudden decrease in cooling. A real-time calculation of vapour quality would allow the design of leaner cooling systems as dry out conditions can be observed before they occur, reducing the safety factors taken in sizing the liquid mass of the system.

Vapour quality at any point on a P-h diagram can be determined using the lever rule inside the vapour dome. In 2PACL, the challenge is mapping the fluid's exact location. In pure liquid, any point on the P-h diagram can be determined from pressure and temperature, but in phase transition these values are saturation conditions, and therefore a third variable is needed. One obvious choice is density, as shown in Figure 1.3. By knowing the local pressure and density, the exact point in the vapour dome, and therefore the vapour quality, can be determined.



Figure 1.4: The Krohne Optimass 6400 mass flow meter.

1.4 The Krohne Optimass 6400

The Optimass 6400 is a new twin bent tube coriolis mass flow meter. It features 3 independent measurements, from which it calculates 7 output signals. The 3 fundamental measurements to be assessed are:

- Mass Flow Rate - Coriolis principle.
- Density - Natural frequency of an oscillating tube.
- Temperature - Internal probe.

The instrument is unique because of its Entrained Gas Management - it is able to continue reading mass flow, density and temperature of 2-phase flow. The instrument's accuracy has been measured using liquid water and air bubbles, but never with a single fluid in 2 phases.

1.5 Aims, Objectives and Documentation

This study is an initial evaluation of the Optimass 6400's steady-state measurement accuracy over a wide operating envelope. Its aim is to evaluate and validate the strategy for determining vapour quality, quantify the attainable measurement under various conditions, and identify performance trends and areas for further research. Specific goals are given below:

- Compare mass flow and density readings with reference instrumentation and theory over a range of temperatures and vapour qualities.

- Quantify the instrument's steady-state performance and, if possible, identify an effective performance envelope.
- Express the instrument's accuracy in terms of vapour quality.
- Investigate the physical phenomena behind any performance trends.
- Identify areas for further research.

This report documents the background to the problem and relevant literature in Chapter 2, describes the method employed to test and analyse the sensor's performance in Chapter 3, and the results of the testing in Chapter 4. Further, it documents speculation as to the cause of performance trends revealed in Chapter 4 and identifies areas for further research in Chapter 7.

2. Literature Review

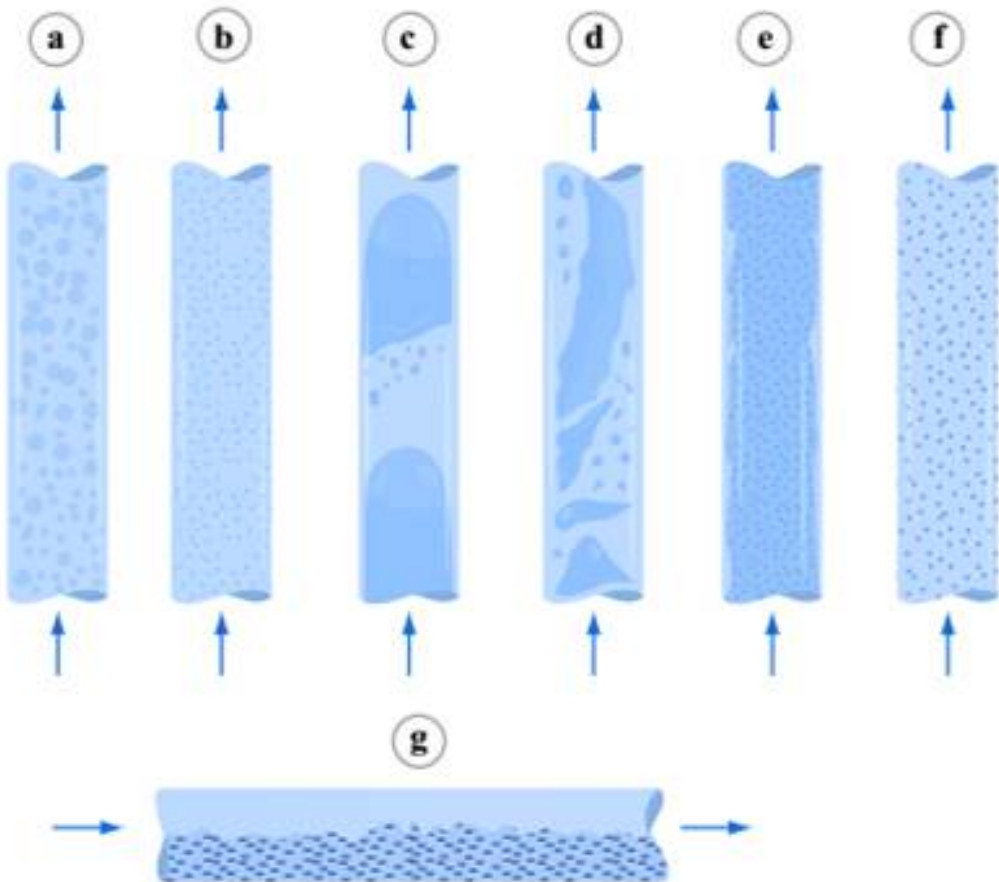
2.1 Behaviour of 2-Phase CO₂

As a coolant, CO₂ is new and different from conventional refrigerants, and its characteristics are generally difficult to predict. Research so far has characterized its performance in terms of heat transfer coefficients in convection and boiling, pressure drops and flow pattern. These phenomena are characterised with respect to vapour quality, because this convenient parameter takes into account mass flow rate and heat flux, simplifying data visualisation. A recent statistical review presented by Mastrullo et al. updated existing data sets with new experimental data, improving the characterisation of this coolant. [4]

The most relevant data to this study concerns flow patterns. As a flowing coolant evaporates, it transitions through various physical configurations, some of which are summarised in 2.1. These flow patterns are influenced by the vapour quality of the fluid, the mass flux - a function of mass flow rate and pipe geometry, and the presence of swirl or turbulence.

Cheng et al. published a widely-cited flow pattern map based on the previous Cheng-Ribatski-Wojtan-Thome relations. [13]. The map, shown in Figure 2.2, is valid for tube diameters between 0.6 and 10 mm, and mass velocities between 50 and 1500 kgm⁻²s⁻¹, making it relevant to the present study.

While the boundaries between flow regimes are frequently updated with new data, the general pattern of CO₂ cooling performance as it evaporates has remained consistent. A broad spectrum of literature summarised in a review by Mastrullo et al. [4] observes the flow transitioning from single-phase to some form of intermittent flow, then to a broad region of annular flow, then finally to dry out, where it exhibits a dramatic decrease in HTC and thus in cooling efficiency. If the coolant continues to be heated, it reaches mist flow, and its cooling performance continues to plummet.



Typical configuration of (a) bubbly flow, (b) dispersed bubbly (i.e. fine bubbles dispersed in the continuous liquid phase), (c) plug/slug flow, (d) churn flow, (e) annular flow, (f) mist flow (i.e. fine droplets dispersed in the continuous vapor phase) and (g) stratified flow. Note: mist flow is possible only in a heated channel; stratified flow is possible only in a horizontal channel.

Image by MIT OpenCourseWare.

Figure 2.1: A summary of liquid-vapour flow patterns. [24]

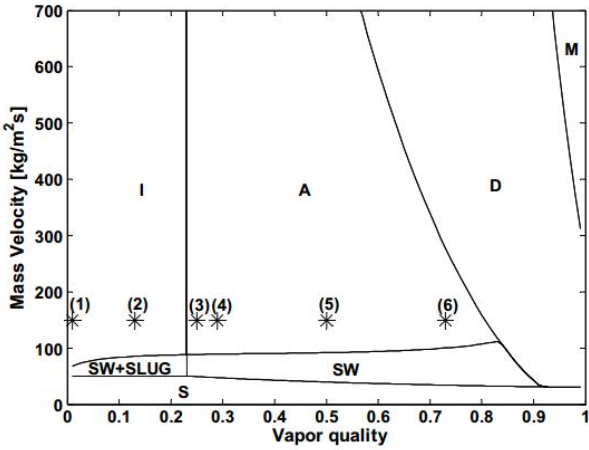


Figure 2.2: The updated flow pattern map for CO₂ developed by Cheng et al. [13]

2.2 Determining Vapour Quality

Literature on direct measurement of vapour quality is scarce, especially for CO₂. B.R. Jean presented a steam quality sensor that employs microwaves, yielding an accuracy of 2.8%. [29]. The operating principle relied on the dielectric properties of water. A review of steam quality measurement approaches conducted by Dorman and Fridman [30] evaluated calorimeter, chemical tracer and flow separation methods, revealing their significant drawbacks. The authors then presented a new theoretical method for measuring vapour fraction, but it was limited to fluid in a static container.

Void fraction, defined as the volumetric fraction of fluid in the vapour phase, is an intuitive candidate for an indirect measurement of vapour quality.

$$\phi = \frac{V_{vapour}}{V_{fluid}} \quad (2.1)$$

Indeed, several methods have been developed for the measurement of void fraction, relying on capacitance measurement [27], x-rays [26], electron sources [23] and gamma ray densiometers [25]. However, the conversion of void fraction to vapour quality is far from straightforward, as the mass fraction of vapour depends on the density of both the vapour and the fluid:

$$X = \phi \frac{\rho_{vapour}}{\rho_{fluid}} \quad (2.2)$$

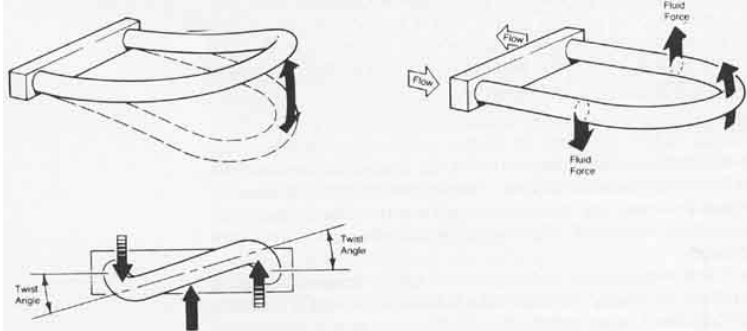


Figure 2.3: The working principle of coriolis flow meters.

Empirical relations have been developed, most notably by Zuber and Findaly, between void fraction and vapour quality, but their complexity and limited range makes them impractical for a real-time application.[28]. As mentioned in Section 2.1, vapour quality is a common parameter across combinations of mass and heat flux, and it is therefore favoured by researchers in the characterisation of CO₂. Research of flow patterns, heat transfer coefficients and 2-phase pressure drops employs vapour quality as a key variable for the visualisation of data. [13][8].

Because the direct measurement of vapour quality is not practical, these researchers have relied on analytically determining vapour quality from test conditions. Most have evaluated the enthalpy of the fluid in a sub-cooled liquid state, before applying a measured heat load. Given the heat load and the mass flow rate, they are able to calculate the corresponding change in enthalpy, giving the 2-phase enthalpy and therefore the vapour quality. [5] [3] [6] Details of this approach are given in 3.

2.3 2-Phase Performance of Coriolis Flow Meters

Coriolis flow meters work by inducing a phase shift in the forced oscillations of two bent tubes using the Coriolis principle. A schematic of the principle is given in figure 2.3. As the tubes vibrate at their natural frequency, the velocity of the flow as it is directed radially toward and away from the axis of oscillation in the bent sections induces a phase shift varying linearly with the mass flow rate of the fluid through the instrument. [7][1]

Density, when independently measured in coriolis flow meters, is typically determined from the resonant frequency of the bent tubes. [7][1] The frequency is a function of the tube stiffness and mass. So any change in mass reflects a change in density of the fluid inside the tube. The sensor corrects for temperature effects on stiffness and, with a known tube volume, determines the density. [7]

Both of these measurement principles can be severely disrupted by 2-phase flow. Entrained gas may create slip planes between the phases, which cause unpredictable forces and vibrations.[7][21][31] This leads to two problems in instrumentation: first, the unexpected vibrations disturb sensitive electronics. Second, the slip between the phases dampens forced vibrations, possibly stopping the sensor from reading altogether. In a typical coriolis flow meter, the first symptom of entrained gas is the drive gain, the power required to force the tubes' oscillation, rising to 100%. [7][18]

Some manufacturers of process instrumentation have developed products to detect entrained gas. The Emerson Rosemount 3051S Pressure Transmitter, for example, employs statistical methods to detect characteristic frequencies of entrained gas. [20]

Because both the mass and density measurements in coriolis flow meters rely on macroscopic properties of the fluid - flow velocity and aggregate density, intermittent flow intuitively seems the most problematic for these instruments. It can be imagined that a sudden pulse of high-velocity gas between normal liquid phases could seriously disrupt sensitive electronics. Indeed, the ISO standard for coriolis meters indicates that they can be used without problems in pure gas-phase flow as well as in homogeneous 2-phase mixtures - an annular flow pattern, for example. [7] The obscure industrial research on this topic confirms this trend with many manufacturers stating that annular flow patterns can be measured accurately. [31]

What makes the Optimass 6400 unique is its Entrained Gas Management technology. The meter itself is a copy of the older Optimass 6000, but innovations in the MFC 400 signal converter that it interfaces with set it apart. These electronics employ advanced signal processing and a completely digital drive signal to allow the instrument to continue measuring in 2-phase flow. [12][21]

3. Methods

3.1 Experimental Methods

Laboratory research was carried out using the future CMS pixel detector cooling system located in the Tracker Integration Facility clean room at CERN. This cooling system, hereafter referred to as *TIF*, employs the *2PACL* concept for evaporative CO₂ cooling. It allows active control of the coolant temperature, its flow rate and the heat load applied to it.

TIF consists of a membrane pump routing liquid CO₂ through a concentric transfer line to a manifold where the flow is split and can be heated. *Dummy Load* heaters represent the detector heat load, evaporating the CO₂ in the manifold. An accumulator containing 2-phase fluid on the return line of the manifold regulates the pressure set point using an array of heaters and a heat exchanger. A freon chiller cools the accumulator and the condenser at the pump inlet.

A full Process and Instrumenation Diagram is given in Appendix A.

3.1.1 Apparatus

The TIF cooling system services eight cooling loops in the manifold and includes several bypasses, heaters and instrumentation that are mostly relevant to the start-up procedure. These are configured using a series of pneumatic, manual and electro-mechanical valves. The plant was configured the same way for all tests: with all bypass loops closed, and a single loop, number 7424, open in the manifold. This configuration ensured all fluid leaving the plant passed through this loop and through the Optimass instrument, and allows the experimental apparatus to be represented by a simplified P & I diagram given in Figure ???. The Optimass instrument was mounted on a test stand close to the *TIF* manifold, as shown in figure 3.3a. Following guidance from Krohne, it was mounted upside-down, with the MFC 400 signal converter closer to the floor. The instrument's discharge was connected through a flexible pipe to the the return lines of loop 7424 in the *TIF* manifold. On the supply side, the instrument was connected directly to the discharge of the heating section. The heating section of loop 7424 consists of a 35 mm OD vertical pipe welded to two tee unions.

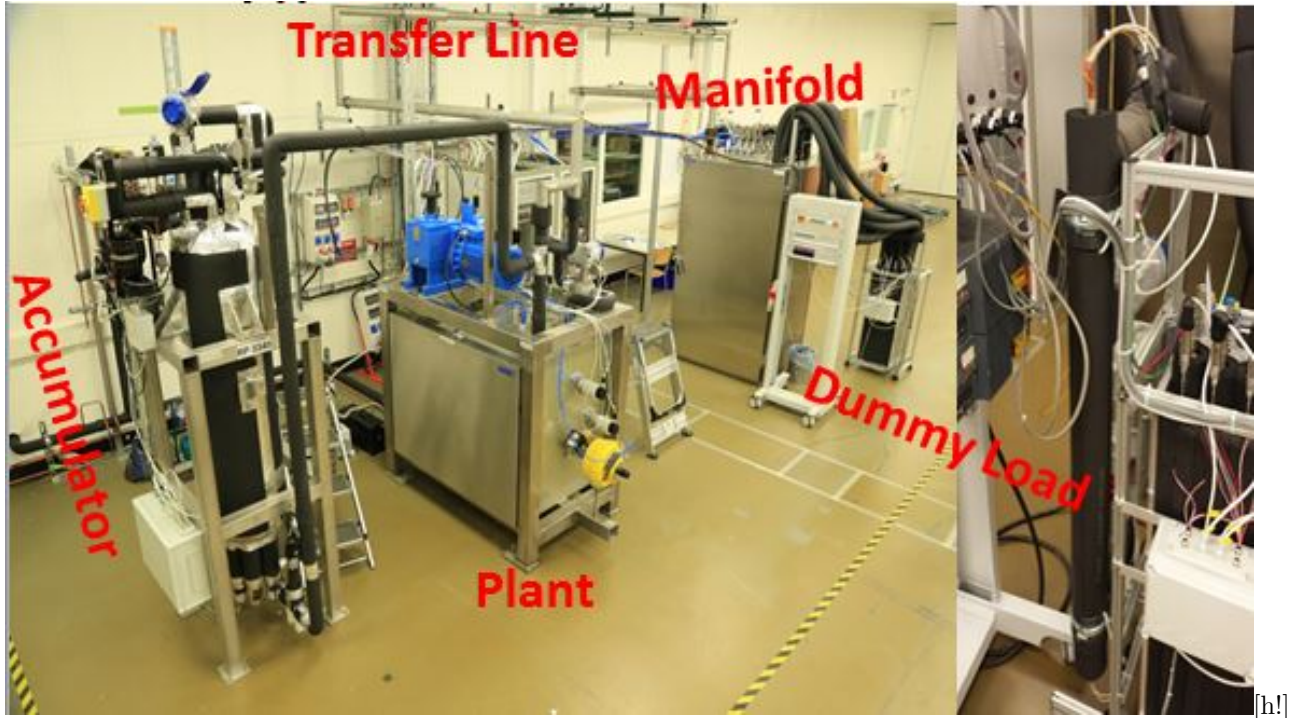


Figure 3.1: The TIF cooling plant[L] and dummy load heater [R]. [19]

Two cartridge heater inside 22 mm pipes are axially inserted into the pipe through the tee fittings, as shown in figure 3.3b and in the drawing in Appendix C. The flow enters the heating section radially with respect to the heaters through the lower tee union. It is forced into an annular shape encircling the heater, and flows upward to the discharge tee-union. It then enters a short unobstructed series of circular fittings before reaching the Optimass instrument. Guidance from Krohne engineers and the instrument documentation indicated that the geometry at the sensor inlet was satisfactory. The vacuum-insulated instrument, as well as all exposed piping, was covered with a 20 mm layer of *Armaflex* insulation to mitigate heat pick-up. All fittings were leak tested at 50 bar gas using a CO₂ sniffer prior to testing, and the instrument's position and inlet conditions respected the guidelines given in Appendix, as well as input from Krohne engineers.

3.1.2 Control and Data Acquisition

All of the instrumentation on the TIF plant, the dummy load and the Optimass flow meter is cabled to a central PLC in the TIF clean room. Each instrument communicates a 4-20 mA analogue signal, which is mapped by the PLC to produce a value in the correct units. All of the data is continuously logged to a server, day and night. The data is logged using a change or duration algorithm - logging new data only when one of the signals has changed. This produces a sampling rate of several Hz during transient conditions - meaning hundreds of thousands of data points over the 3-week test campaign. The Optimass sensor was

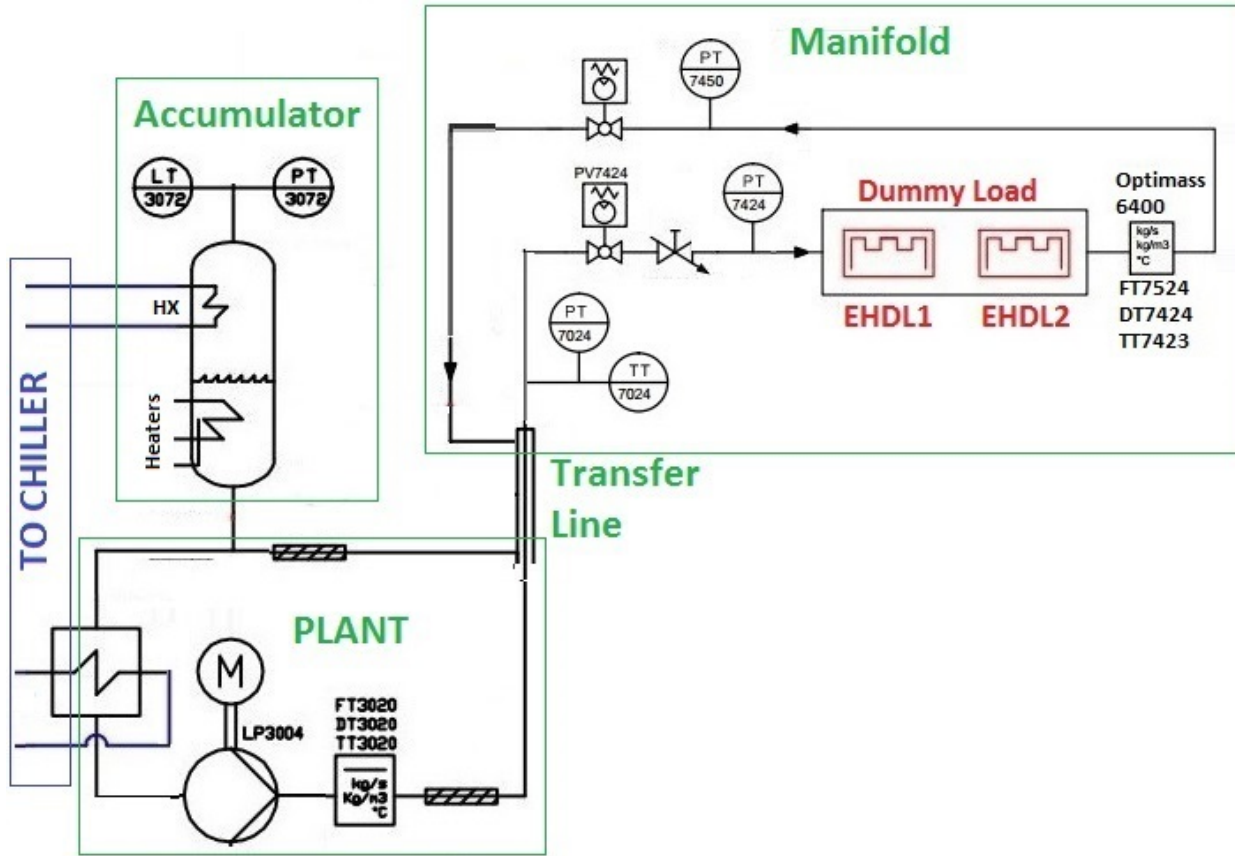
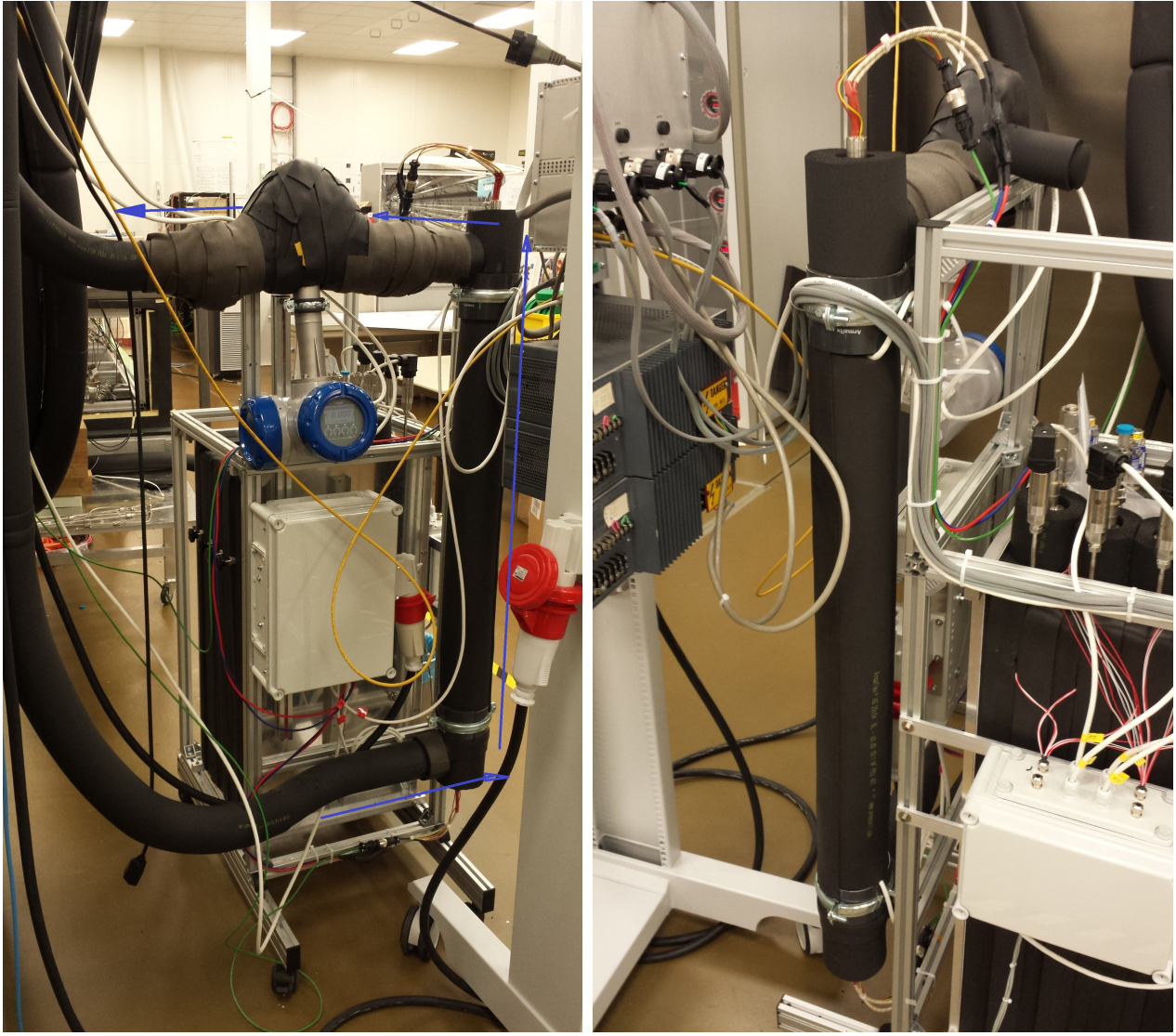


Figure 3.2: A simplified process and instrumentation diagram of the TIF cooling plant in the configuration relevant to the tests, displaying only relevant instrumentation. A diagram of the whole TIF is given in appendix A.



(a) Front view.

(b) Side view.

Figure 3.3: Photographs of the Optimass sensor connected to the dummy load heating section. The direction of flow is given by the blue arrows.

configured by Krohne Italy to deliver mass flow, density and temperature signals through a 4-20 mA bus in the following measurement ranges:

- Mass Flow Rate: $1.4\text{-}115 \text{ gs}^{-1}$
- Density: $100.6\text{ - }1100 \text{ kgm}^{-3}$
- Temperature: $-40\text{ - }+40 \text{ }^{\circ}\text{C}$

The sensor was cabled to the same PLC controlling TIF and logging all of its instrumentation, and the signals were mapped to the values configured by Krohne. This approach streamlined control and post-processing by consolidating the plant, heaters and instrument on a single Scada interface, and logging the data in a single location at common timesteps.

3.1.3 Variables and Assumptions

The instrument's performance was to be assessed in relation to three independent variables:

- Coolant temperature - regulated by the accumulator set point.
- Mass flow rate - set by the pump speed and stroke.
- Heat Load - set by the heaters' rms current.

The coolant temperature set point determines the position along the vapour dome on a P-h diagram of the 2PACL cycle, and therefore the local pressure in the instrument. This influences the evaporative behaviour of the coolant, as well as the vapour quality for a given density. While a wide range of temperature was to be explored, the invariance of the temperature during a tests was an essential control variable.

The mass flow rate was set by the speed and stroke of the pump, but not regulated during tests. This meant that as the vapour quality of the coolant increased, the resultant increase in pressure drop decreased the effective flow rate for given pump conditions. The resulting fluctuations in true flow rate affect the trends plotted by nominal flow rate, but because flow rate is measured in real time, they did not effect error signal calculations.

The dummy load heaters are resistive cartridge heaters, whose power is controlled by pulse width modulation. The user specifies a Watt value on the Scada interface, and the PLC applies the correct PWM signal to achieve the demand power output. Heater control is open-loop, but their performance has been validated in the past.

A broad range of all three variables was explored. But because this experiment sought only to evaluate

Key Variables and Settling Times		
Variable	Control Method	Settling Time
Temperature	Accumulator Set Point	30-90 minutes
Mass Flow Rate	Pump speed and stroke	15-30 minutes
Vapour Quality	Dummy Load Power	5-15 minutes

Table 3.1: Key variables, their control method and their settling times.

steady-state performance, transient data was to be minimised. The control variables were therefore closely monitored to minimise fluctuations.

3.1.4 Test Protocol

Before beginning 2-phase testing, the instrument's calibration was validated in pure liquid by comparing its readings of mass flow, density and temperature with a reference instrument on the plant (FT3020) for a range of flow rates and temperatures.

For 2-phase testing, a test protocol was developed to ensure consistency of data. A change to any of the independent variables caused a significant transient response. But the process of fine-tuning the values and waiting for their response to settle differed for each variable. Tests were designed accordingly.

Altering test conditions employed a nested approach. First, the coolant temperature was set in the accumulator. Then various heat loads were applied at a given pump speed to explore a range of vapour qualities at a given flow rate, before changing the pump conditions. A typical test segment: various heat loads at a given flow rate and temperature, is shown in Figure 3.4.



Figure 3.4: A typical test. The steps in heat load are shown as vertical red lines.

3.2 Data Analysis Methods

A method, summarised in Figure 3.5, was devised for the export, pre-processing and process of data. This approach filtered through the hundreds of thousands of data points to reach a small subset of steady-state data during test conditions.

3.2.1 Export Pre-Processing

Including time, 12 signals out of the dozens logged in the PLC were identified as being key for this study. These are summarised in table 3.2.

A page of plots tracking these signals was created in the Scada interface. Then, .csv data for each signal was exported by navigating to the time of a given test and exporting a 4 hour window of data. These .csv files for each day of testing were then pre-processed using modified MATLAB scripts developed by Bart Verlaat. Pre-processing involved merging the data from each test into a single database, handling empty cells and

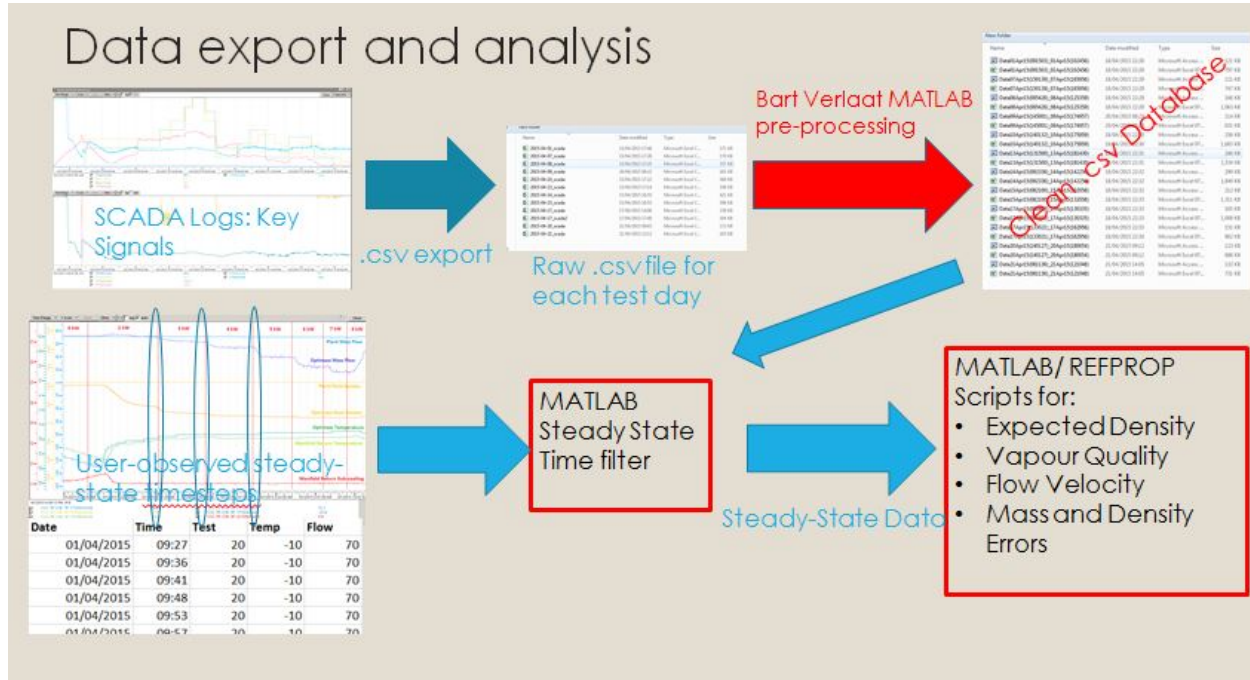


Figure 3.5: A summary of data processing and analysis.

Key Signals			
Signal Type	Signal Name	Thermodynamic Symbol	Description
	FT7524	\dot{m}	Mass flow rate measured by Optimass 6400
Optimass	DT7424	ρ_5	Density measured by Optimass 6400
	TT7424	T_5	Temerature measured by Optimass 6400
Reference	FT3020	\dot{m}_{ref}	Liquid mass flow rate measured in plant.
Reference	PT7024	P_3	Manifold supply pressure.
Reference	TT7024	T_3	Manifold supply temperature.
Reference	EHDL1	\dot{Q}_a	Dummy load heater 1 power.
Reference	EHDL2	\dot{Q}_b	Dummy load heater 2 power.
Reference	PT7450	P'_5	Pressure at instrument discharge.

Table 3.2: Key Signals

overlapping timesteps, and saving the cleaned data in a new database to be called by MATLAB.

3.2.2 Data Processing and Visualisation

With the key signals filtered to leave only steady state conditions, these were processed to assess the sensor's performance. The sensor was evaluated by comparing its readings to a combination of reference instrumentation and analytically computed reference conditions.

Analysis employed an theoretical MATLAB model to compute thermodynamic state variables in the sensor, and called a refrigerant simulation program called REFPROP to compute the local conditions of interest. REFPROP, developed by National Instruments, is a widely used program that simulates refrigerant performance using a combination of analytical and empirical methods.

3.2.3 Calculation of Reference Conditions

The local density and vapour quality in the Optimass sensor were calculated using the local pressure and specific enthalpy. A pressure and an enthalpy give the fluid's exact location in the vapour dome, and the vapour quality and density can be read from the chart, as shown in Figure ???. This was implemented using REFPROP. With the following syntax:

$$Q = refpropm('Q', 'P', < P_5 [kPa] >, 'H', < h_5 [J/kg] >, 'CO2')$$

The local enthalpy at the sensor, h_5 , is given by the sum of the manifold inlet enthalpy, h_3 and the change in enthalpy due to the heat load, Δh .

h_3 was determined with REFPROP from the inlet manifold inlet conditions (Pressure and Temperature in pure liquid), while the change in enthalpy was calculated from the heat load and reference mass flow rate.

$$h_3 = refpropm('H', 'P', < P_3 [kPa] >, 'T', < T_3 [K] >, 'CO2')$$

$$p = \text{Heat Load [W]}$$

$$\Delta h = \frac{p}{\dot{m}} \quad (3.1)$$

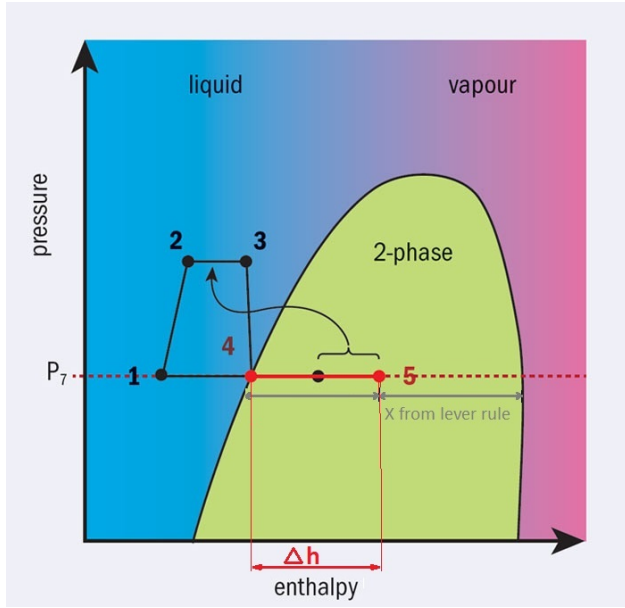


Figure 3.6: The analytic model for calculating local 2-phase conditions at the flow meter.

3.3 Calculation of Vapour Phase Velocity

The vapour phase velocity is a relevant parameter to flow meter performance, representing the linear velocity of the vapour phase in the pipe. The VPV depends both on the vapour quality and the density of the vapour phase, which in turn varies with the saturation conditions.

$$X = \frac{\dot{m}_{vap}}{\dot{m}_{fluid}} \quad (3.2)$$

$$VSV[ms^{-1}] = \frac{\dot{m}X}{\rho_{vap}CSA} \quad (3.3)$$

$$(3.4)$$

The difficulty here is determining the vapour phase density from the aggregate density, but this problem was handled with REFPROP:

$\rho_{vap} = \text{refpropm}('Q', <\text{Vapour Quality}>, T, <\text{Saturation Temperature } [^\circ\text{C}]>, 'CO2');$

4. Results

Because of the size of the raw data spread over weeks of testing and the focus of this study on steady-state conditions, the results presented below summarise the sensor's performance by examining measurement errors under various conditions. The key parameters have been defined as the relative flow rate measurement error, and the relative density measurement error. Vapour quality has been adopted as a common parameter to plot performance against, as is common in the research discussed in Chapter 2.

4.1 Overview

Figures 4.1 and 4.2 give an overview of the flow meter's performance in all the conditions tested by plotting relative flow and density errors across a range of vapour qualities. The mass flow errors are largely negative, varying from -100% to 100% and displaying a non-linear relation to vapour quality. The density errors also vary widely, but, for some conditions, their sign changes with vapour quality. The instrument appears to underestimate density in low vapour qualities, and overestimate it at high qualities.

A cursory overview of the errors implies that they are far from predictable, varying non-linearly with vapour quality. Further, the overall performance of the instrument across the range of vapour qualities appears to vary widely with temperature and nominal flow rate.

Despite the wide spread of data, the errors appear repeatable. While individual tests with identical nominal conditions have been lumped into common data series in Figure 4.1, separating them allows an assessment of repeatability. Figure 4.3 shows the relative measurement errors for four independent tests at the same temperature and nominal flow rate. Controlling for one of the test conditions refines the data, and reveals two interesting trends in the relative mass and density errors. They are discussed below.

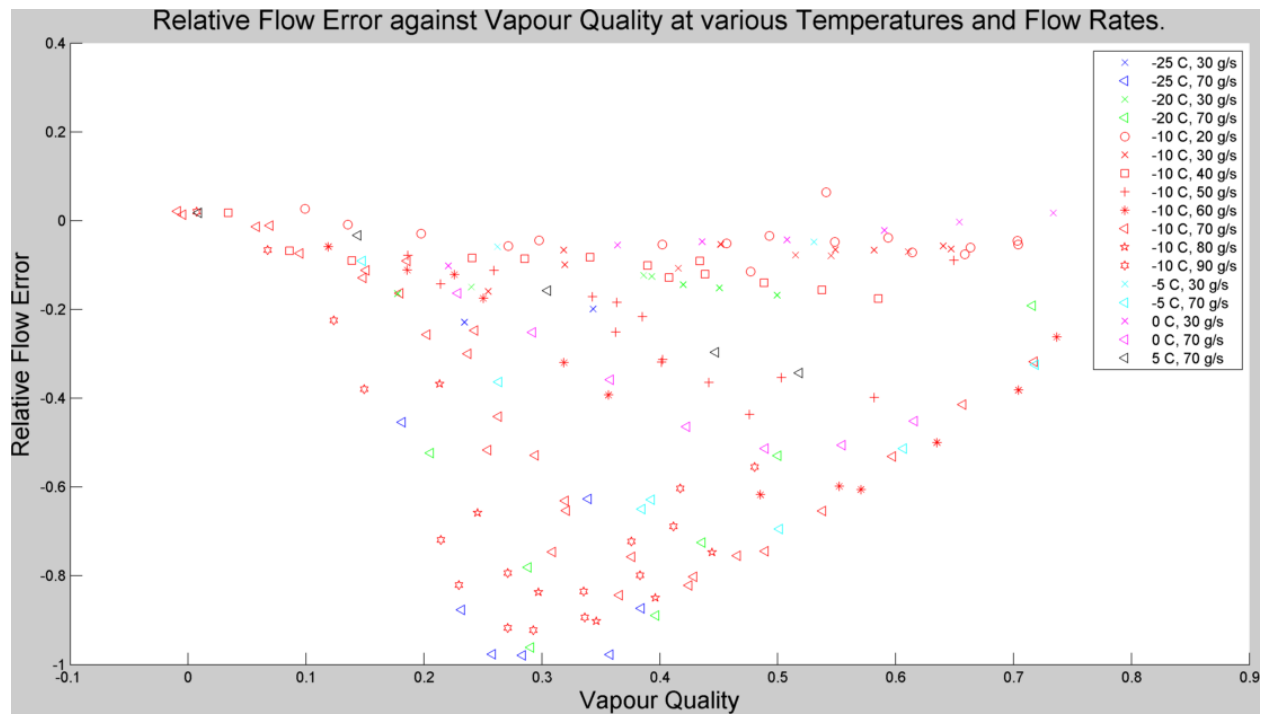


Figure 4.1: An overview of relative mass flow error against vapour quality.

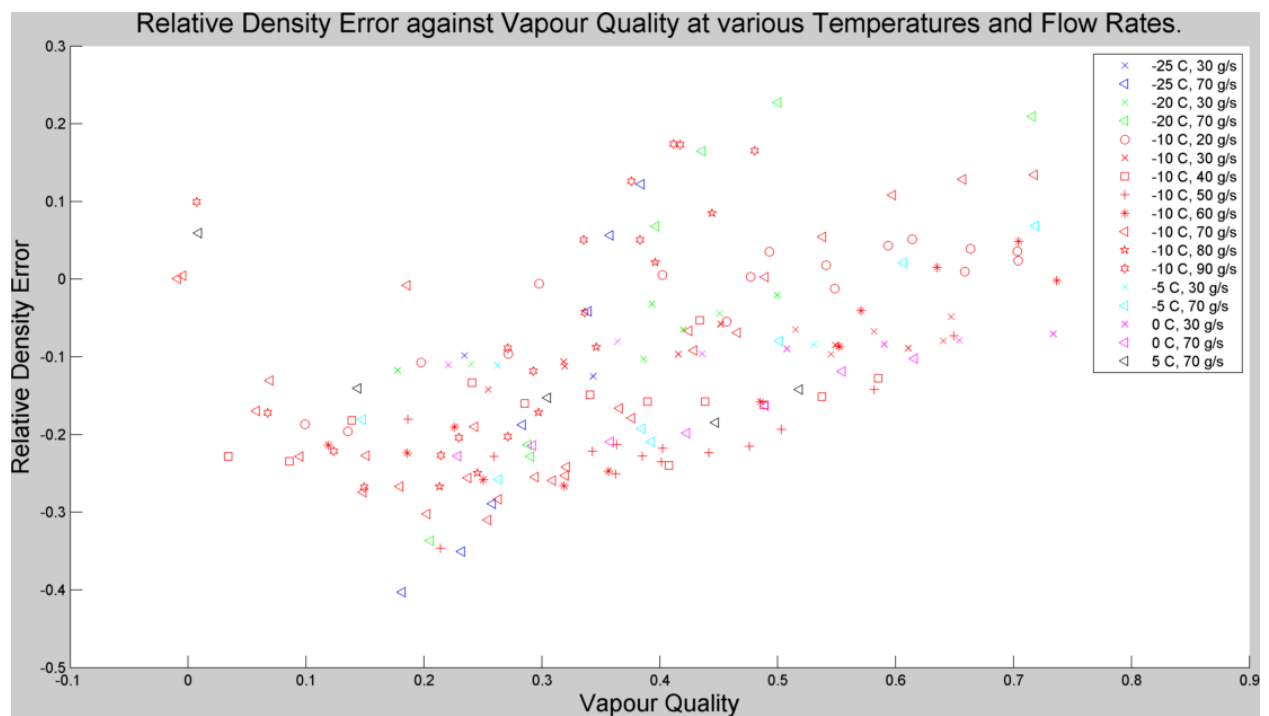


Figure 4.2: An overview of relative density error against vapour quality.

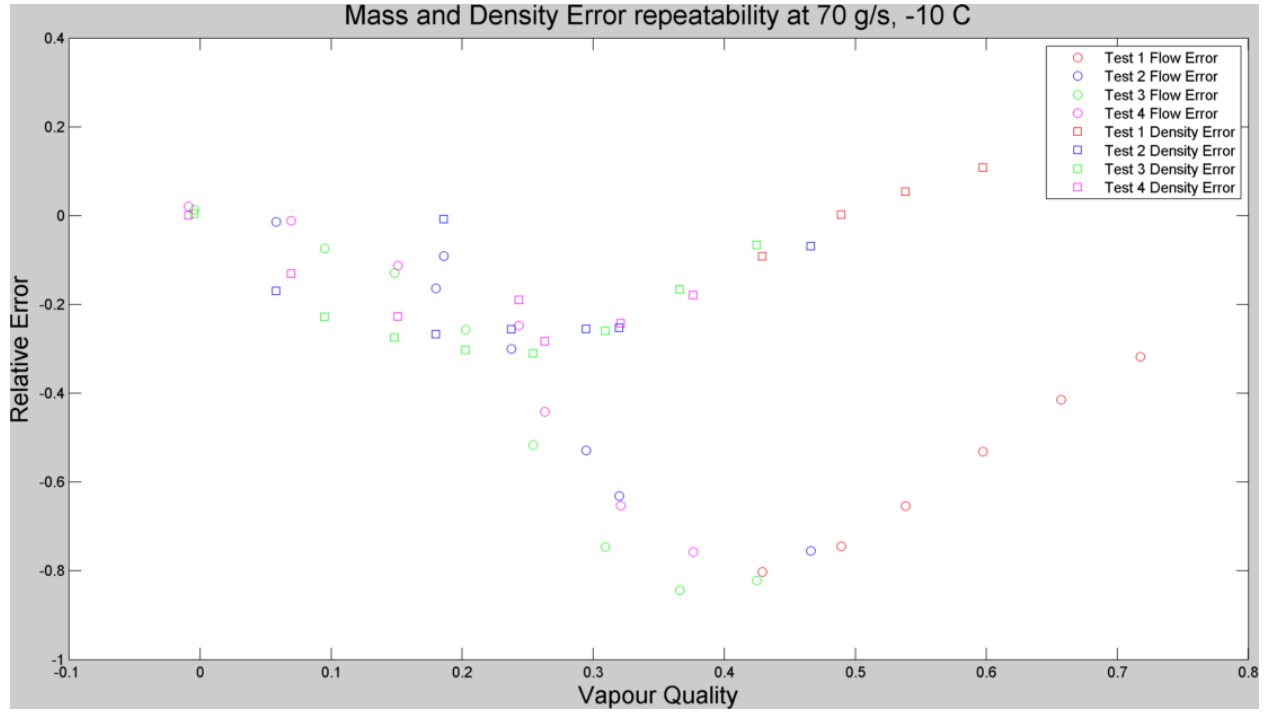


Figure 4.3: Relative mass flow and density errors for various tests at 70 gs^{-1} and -10°C

4.2 Mass Flow Trend

Plotting the relative errors against vapour quality at a single temperature but various flow rates, as in figures 4.4 and 4.5, reveals a clear relation between instrument performance and nominal flow rate. The trends in Figure 4.4, which plots performance for various flow rates at -10°C , show the absolute magnitude of the mass flow error across the entire range of vapour quality increasing with nominal mass flow rate.

In addition, at higher nominal flow rates the magnitude of the mass flow error appears to peak at certain vapour qualities, the peak tending toward dryer fluid as nominal flow rate increases. Both these relations: mean value of the mass flow error, and vapour quality at the peak error can not be immediately explained by the theory. However, two potential explanations are the flow pattern and the vapour phase velocity (VPV) under these conditions. These two parameters have been calculated for the flow conditions at each of the peak mass flow errors, and are summarised in Table 4.1. The method for these calculations is discussed in Section 3.2.

The density errors displayed in Figure 4.5 also demonstrate an improvement in sensor performance as the nominal flow rate decreases. But it appears the relation is more complex than for mass flow error.

Because flow rate is a first order factor of VPV, this velocity generally increases with nominal flow rate for a given vapour quality, as shown in Figure 4.6.

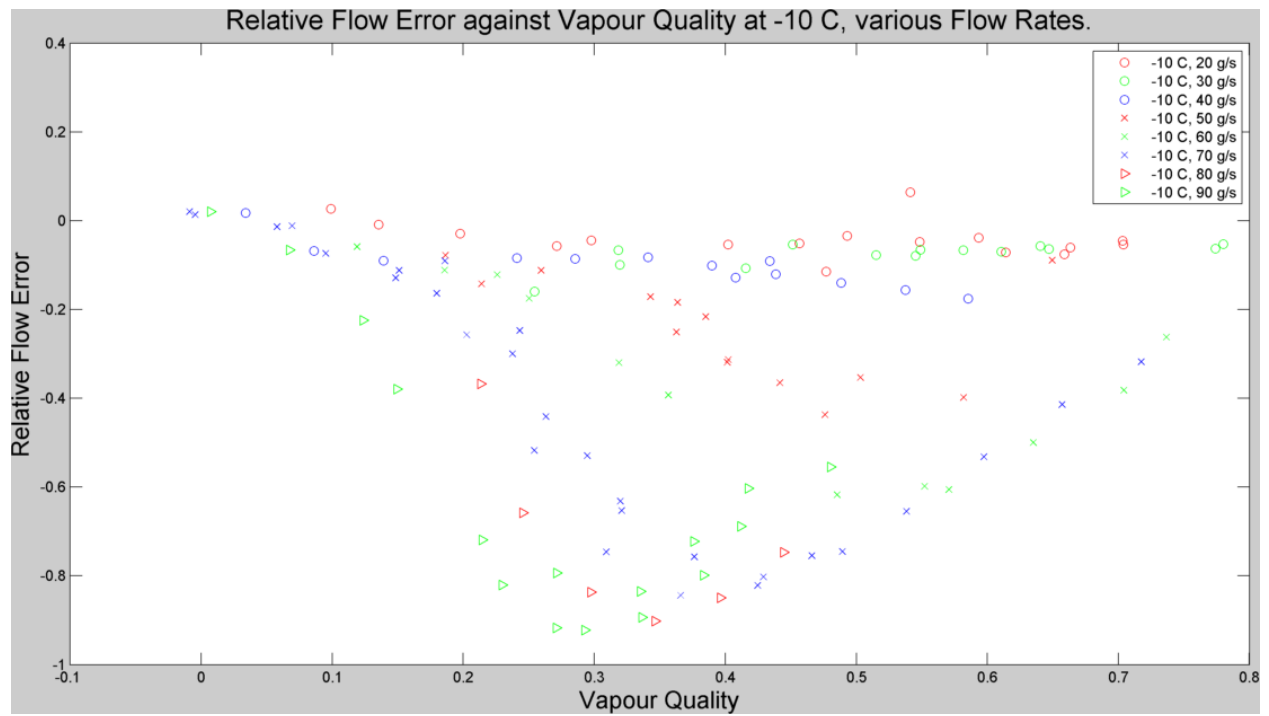


Figure 4.4: Relative mass flow error for several nominal flow rates at -10°C .

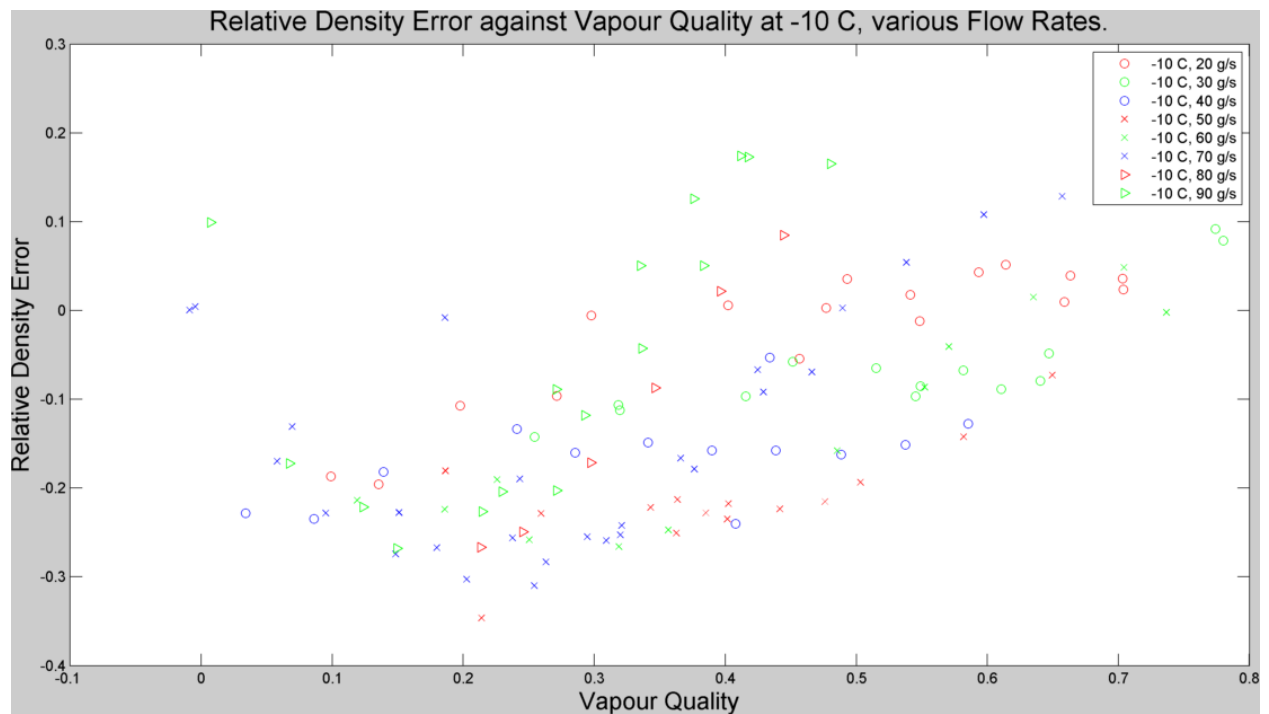


Figure 4.5: Relative mass flow error for several nominal flow rates at -10°C .

Flow conditions at peak mass flow errors for coolang at -10°C				
Nominal Flow Rate	Vapour Quality	Mass Flux	Predicted Flow Pattern	Vapour Phase Velocity
gs ⁻¹		kgm ⁻² s ⁻¹		ms ⁻¹
50	0.476	497	Annular	3.42
60	0.485	597	Annular	3.93
70	0.366	696	Annular	3.90
80	0.346	796	Annular	3.91
90	0.293	895	Annular	3.57

Table 4.1: Flow conditions at peak mass flow errors in 4.4

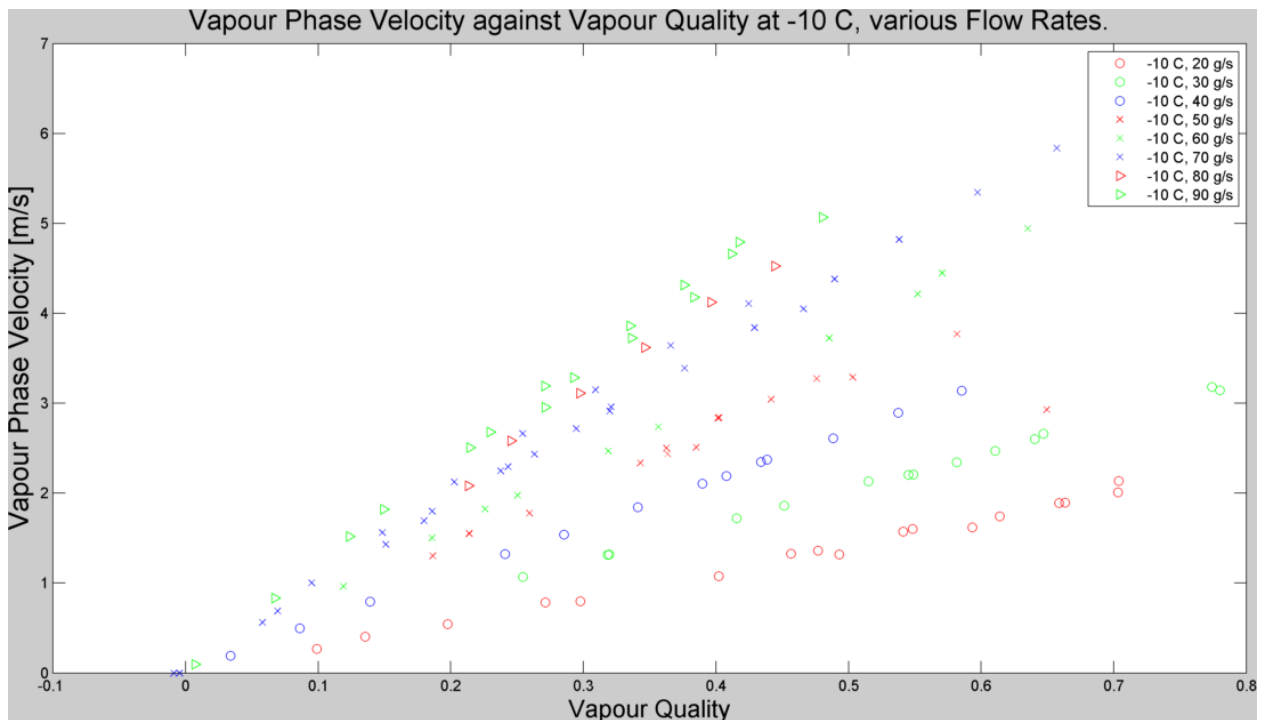


Figure 4.6: Velocity of the vapour phase against vapour quality for various mass flow rates.

4.3 Temperature Trend

A second trend is observable in the data when relative errors-vapour quality relations are plotted for a series of coolant temperatures at a single flow rate, as in figures 4.7 and 4.8. The sensor's performance, both in mass flow and density measurements, generally improves as the coolant temperature increases.

This trend is also visible at lower flow rates, albeit in a less pronounced way. The lower nominal flow rates already exhibit better overall performance but, as shown in figures 4.9 and 4.10, the repeatability of their errors across a range of vapour qualities decreases with coolant temperature.

As with the nominal mass flow rate relation, there is no immediate explanation for the temperature trend. It can be speculated that the so called *reduced pressure* plays a role. This possibility is discussed in Chapter 5.

When expressed in terms of vapour quality measurement errors, the performance of the sensor is encouraging at low flow rates. At 30 gs^{-1} and 20 gs^{-1} , summarised in figures 4.11 and 4.12, the vapour quality error falls within 20%, and decreases with true vapour quality.

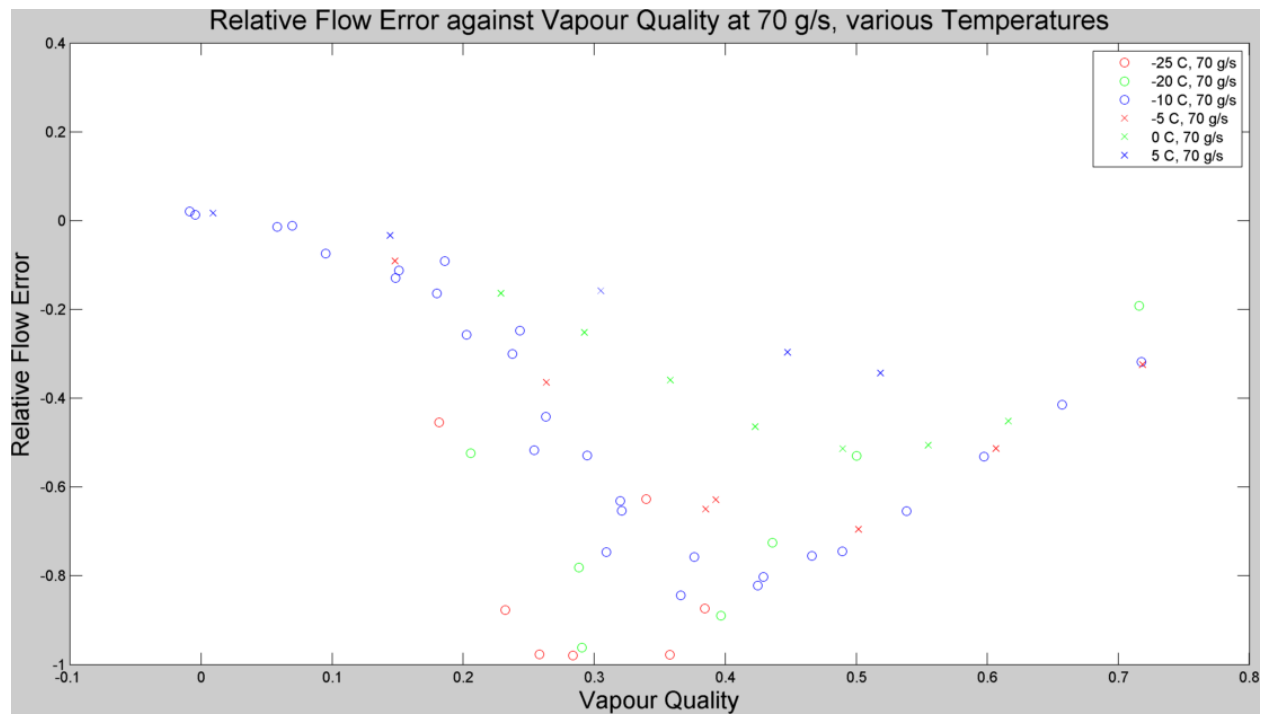


Figure 4.7: Relative mass flow error for several temperatures at 70 gs^{-1} nominal flow rate.

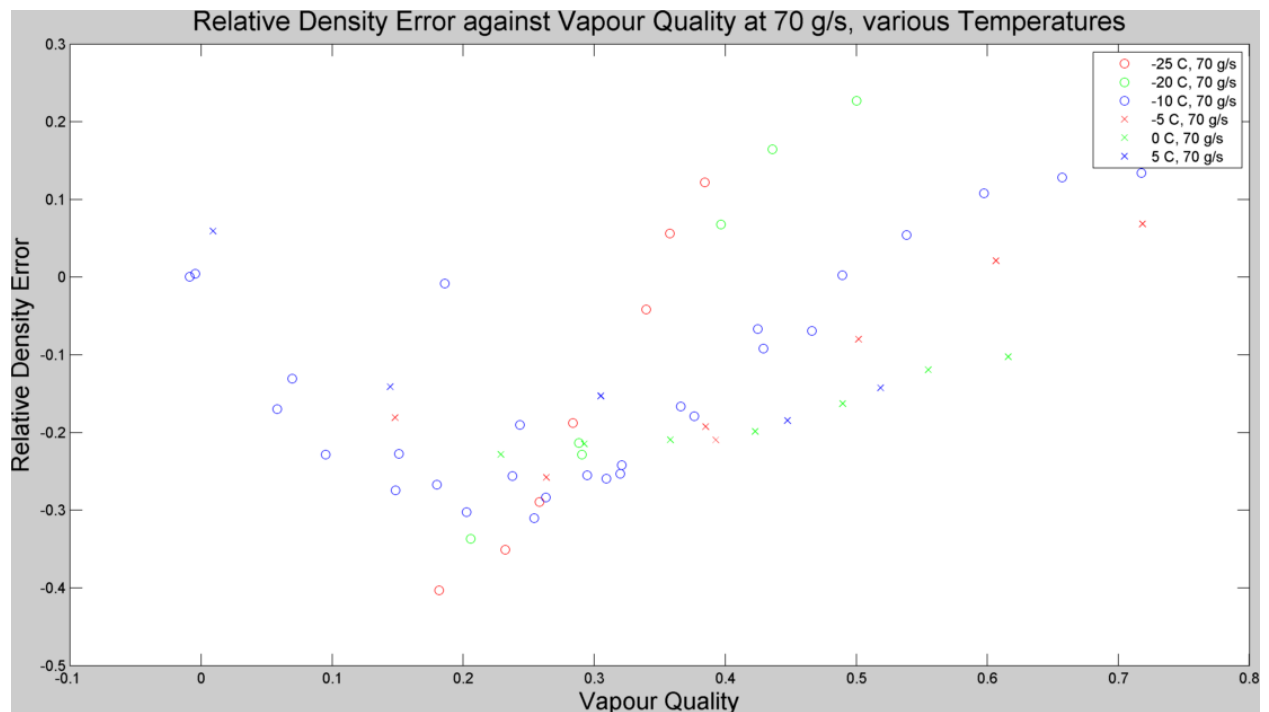


Figure 4.8: Relative density error for several temperatures at 70 gs^{-1} nominal flow rate.

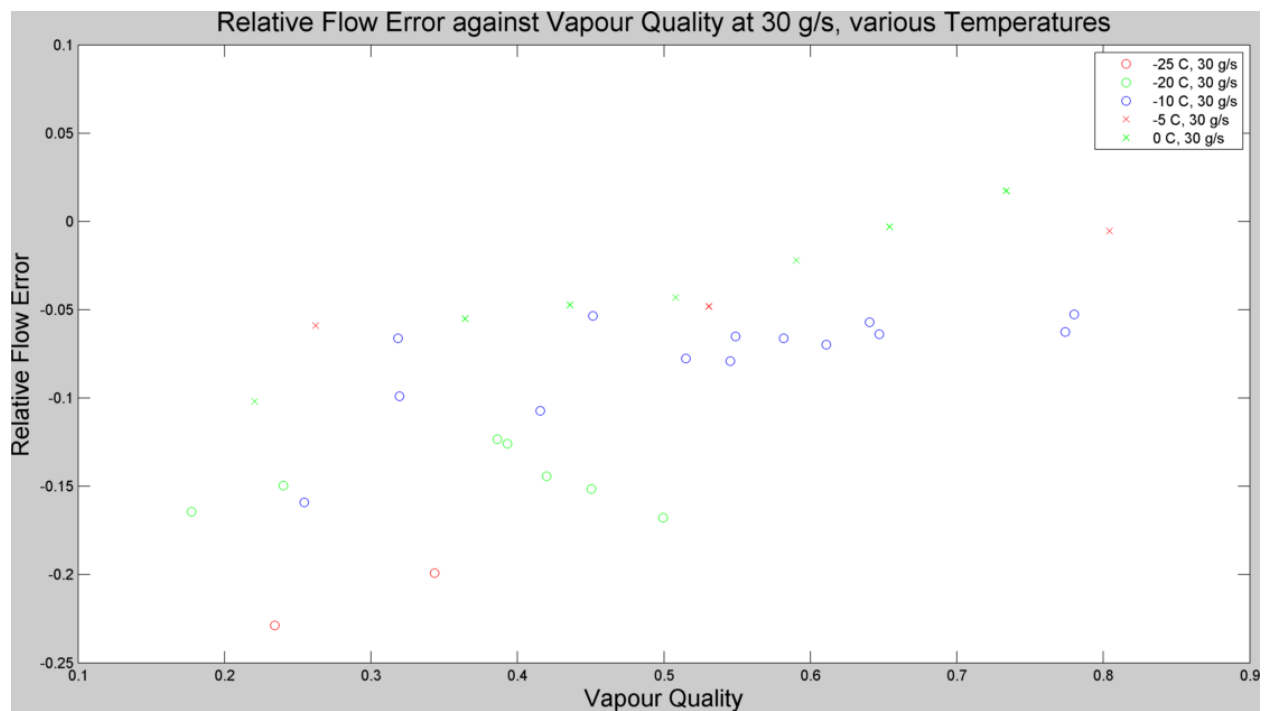


Figure 4.9: Relative mass flow error for several temperatures at 30 gs^{-1} nominal flow rate.

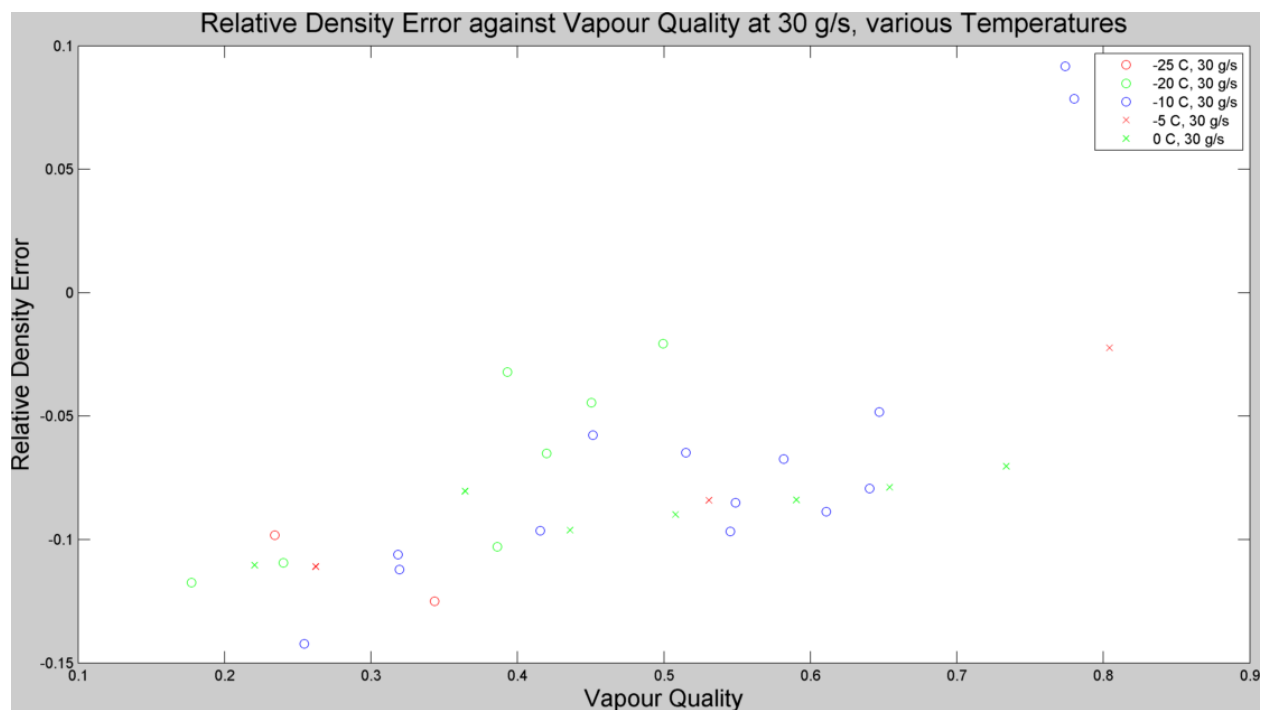


Figure 4.10: Relative mass flow error for several temperatures at 30 gs^{-1} nominal flow rate.

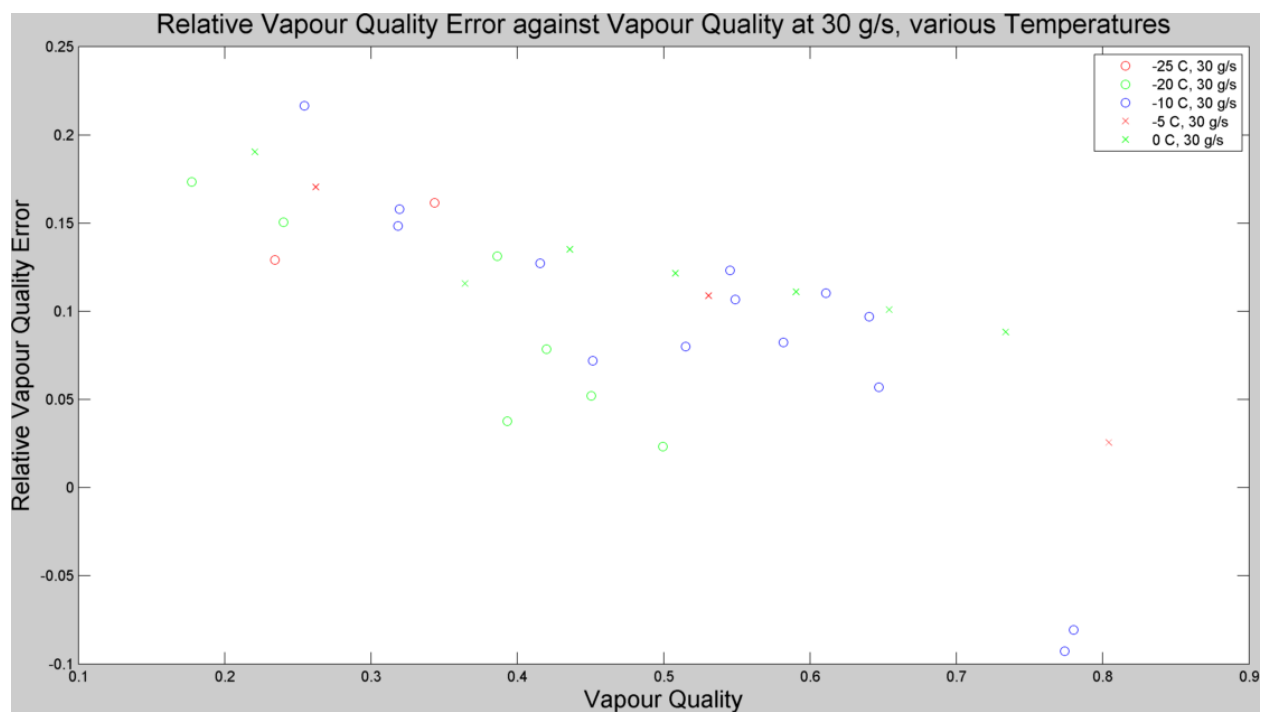


Figure 4.11: Relative vapour quality error against vapour quality for various temperatures at 30 gs^{-1} nominal flow rate.

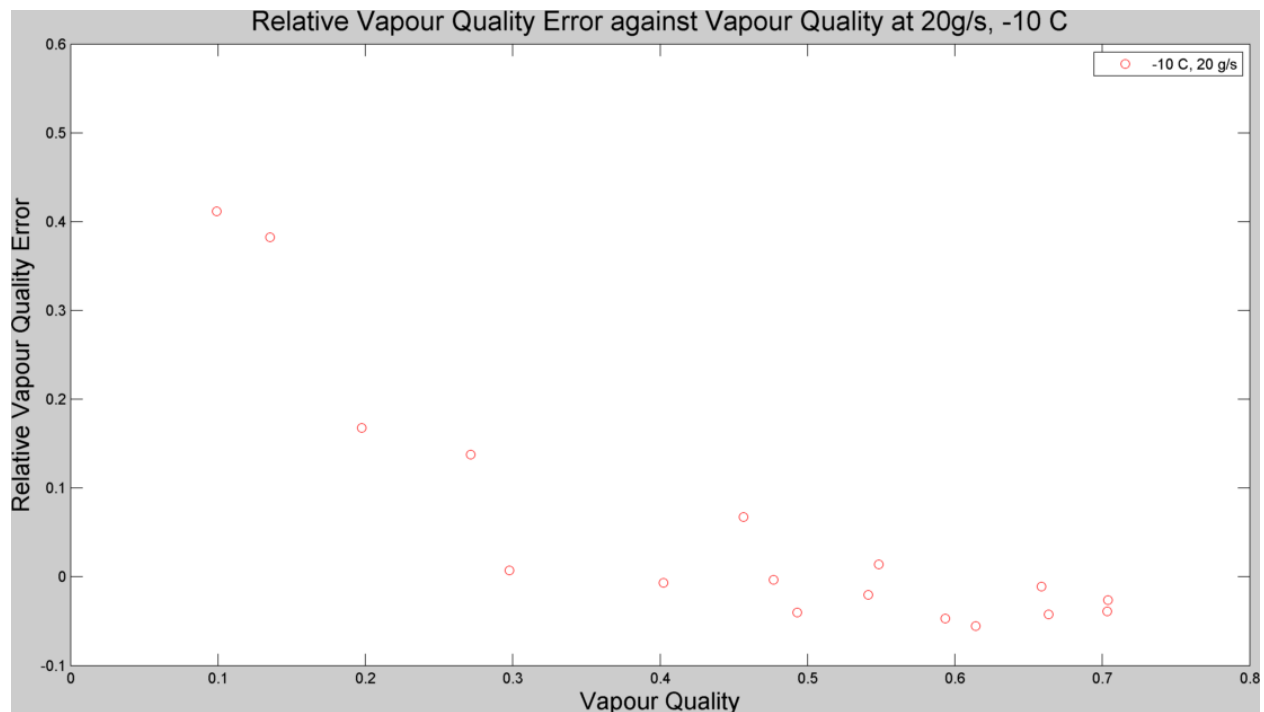


Figure 4.12: Relative vapour quality error against vapour quality for -10°C , 20 gs^{-1} nominal flow rate.

5. Discussion

5.1 Overview

The bulk of results agreed with the intuitive expectations outlined in Chapter 2. While the Optimass 6400 succeeds in continues measurement of 2-phase flow, its performance is unpredictable. Flow and density measurements are complex, and their accuracy seems to depend on temperature, vapour quality and mass flow rate with relations that cannot be readily consolidated into a single theory, given the current literature. While the data is broadly spread, the test method has been broadly validated by its repeatability, and data has been collected strategically to fulfill the original objectives: evaluate a broad performance envelope, identify trends of interest, and conduct further testing to evaluate their repeatability.

In this way, three interesting trends have been identified - at least one of them immediately useful to the potential users of the instrument. First, the measurement accuracy of the instrument of both mass flow rate and density improves as the flow rate is reduced. For the lowest flow rates: 20 and 30 gs^{-1} , the mass flow measurement error magnitude falls within 25%, and within 10% at 20 gs^{-1} . As for density measurement at low flow rates, the instrument's performance is potentially practical for its intended use of estimating vapour quality. At 20 gs^{-1} , the vapour quality measurement error (using the measured density and reference flow rate) decays to less than 10% for vapour qualities greater than 28%. While the error reaches 40% for low vapour qualities, it is at high vapour qualities, close to dry-out, that accuracy is valued. The fact that the instruments accuracy improves to 10% towards the dry side of the vapour means it may perform well enough to be of interest to CERN.

5.2 Mass Flow Rate Trend

The data also demonstrated a second correlation. At -10° , the set point with sufficient flow rates, a clear positive relation between mean value of relative mass flow error and nominal mass flow rate was observed.

In addition, the non-linear mass flow error peaked as a function of vapour quality, with the peaks tending dryward with decreasing flow rate. Given the literature on coriolis flow meter performance in 2-phase, a tempting explanation was the occurrence of a flow pattern transition at this point. To test this, the flow conditions at each of the peak mass flow errors in Figure 4.4 were tabulated in Table 4.1, and their corresponding vapour quality and mass flux were plotted on a Cheng flow pattern map [?]. This revealed that the mass flow error peaks occur at a vapour quality in the order of 10 percentage points greater than the flow pattern transition between intermittent and annular flow predicted by Cheng. In addition, this theory would not explain the dry-ward tendency of the vapour quality at peak mass flow errors with decreasing flow rate.

In response, a second theory for the mass flow trend was explored: the role of vapour phase velocity. Using a MATLAB function calling REFPROP, vapour phase velocities were calculated for the flow conditions at each peak mass flow error and tabulated in Table 4.1. The flow velocities for the peak mass flow rates formed a tight group around 3.5 ms^{-1} , with a standard deviation of: . Given the inexact location of the data points used to approximate the true peaks, this was interpreted as strong evidence that the mass flow error behaviour was due to vapour phase velocity. As shown in Figure 4.6, the vapour phase velocity accelerates with nominal mass flow rate at a given vapour quality, which could explain the increasing magnitude of the mean value of relative mass errors. But crucially, the tight group of vapour phase velocities indicate that the error peaks at a critical velocity, and decays afterward. Because mass flow rate and vapour quality are first order factors of VPV, the VPV reaches critical velocity at a higher vapour quality for a lower mass flow rate. Recall equation ??. This would also explain why the lower nominal mass flow rates do not exhibit a peak error - their VPVs never reach the critical value. As shown in Figure 4.6, the lower mass flow rates do not sufficiently accelerate the vapour phase to reach critical velocity.

5.3 Temperature Trend

5.4 Errors and Uncertainty

The experimental method exhibited sufficient accuracy to deliver clear, repeatable results over a wide range of test conditions. However, the nature of the apparatus limit the relevance of the findings to a preliminary overview of the Optimass instrument's performance. A direct specification of the error bars on the findings is impractical due to the many layers of filtering and analysis, and the assumptions inherent in the physical methodology. TIF is not a laboratory test bench, but a large, operational cooling system. There were significant limitations on the apparatus, including:

- The chiller that cools the accumulator and condenser requires a heat load of at least 3 kW on the system to function effectively, depending on the temperature set point. This makes testing at low flow rates and temperatures at the edges of the plant's envelope difficult. Low flow rates require very low heat loads for a broad range of vapour quality without dry out. And due to environmental heat leak, low temperatures tend to overload the chiller while high ones cause it to overheat.
- Accumulator temperature set point regulation is PID controlled, and responds slowly enough that nominally steady-state data includes temperature fluctuations up to 1 °C.
- The nominal flow rate lacks any control system. It was set by adjusting the speed and stroke of the pump and waiting for the transient response to settle. A change in vapour quality changes the pressure drop and therefore the system characteristic, resulting in flow rate fluctuations in the order of 5 gs^{-1} . All error signals and reference conditions are calculated using the real-time reference flow rate [FT3020], so this error is only in *nominal* flow rate, i.e. flow trends on the plots.
- The inlet pressure at the instrument is a crucial parameter affecting the calculation of reference vapour quality and density. However, the sensor inlet lacks instrumentation. Instead, the pressure in the sensor is assumed to equal the saturation pressure of the temperature measured inside the sensor [TT7424]. Since the flow is 2-phase, it is fair to assume that the saturation pressure is equal to the local pressure. However, a pressure-drop on the inlet side of the instrument would result in an underestimate of true inlet pressure. Krohne specifies a liquid pressure drop in the order of mbar, even at a high flow rates. But there is no data on 2-phase pressure drop, which the literature shows is far higher.

The collective effect of these uncertainties is a study that characterises the overall performance of the Optimass instrument, and demonstrates under which conditions it performs best. While the errors measured are repeatable, the nature of the apparatus means that they are not a reliable measure of the sensor's accuracy under laboratory conditions. As a result, this study is largely a stepping stone: showing the viability of the approach to vapour quality measurement, the conditions underwhich this particular instrument's performance is satisfactory, and areas for futher research.

6. Conclusions

7. Future Work

larger flow meter, dedicated test rig, volumetric flow rate of gas phase? flow regimes, frequency domain analysis, flow meter positioning. real time reference condition calculation. flow velocity. test low flows using bypass. chiller management. definition of true performance envelope. two-phase signal what does it mean?

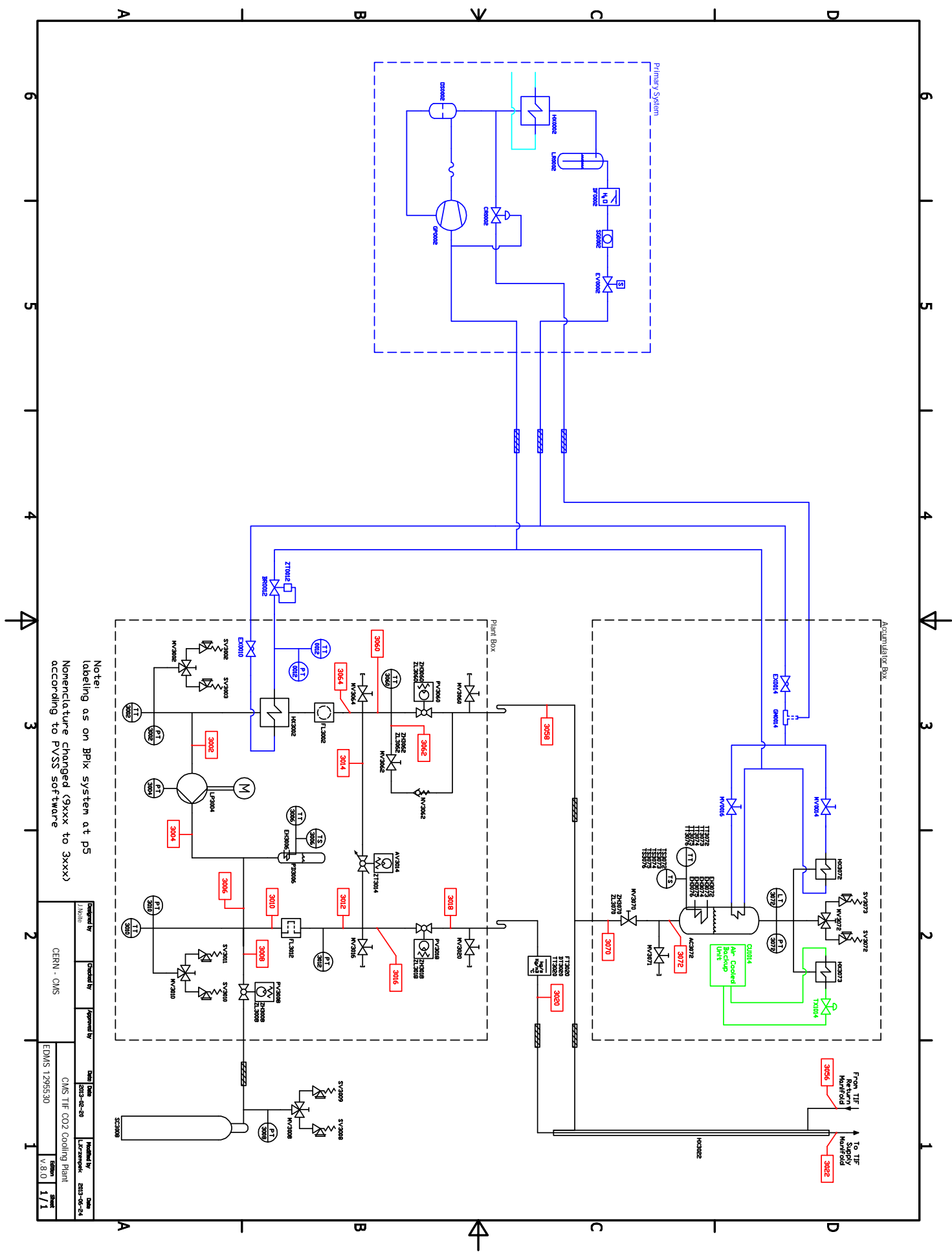
Bibliography

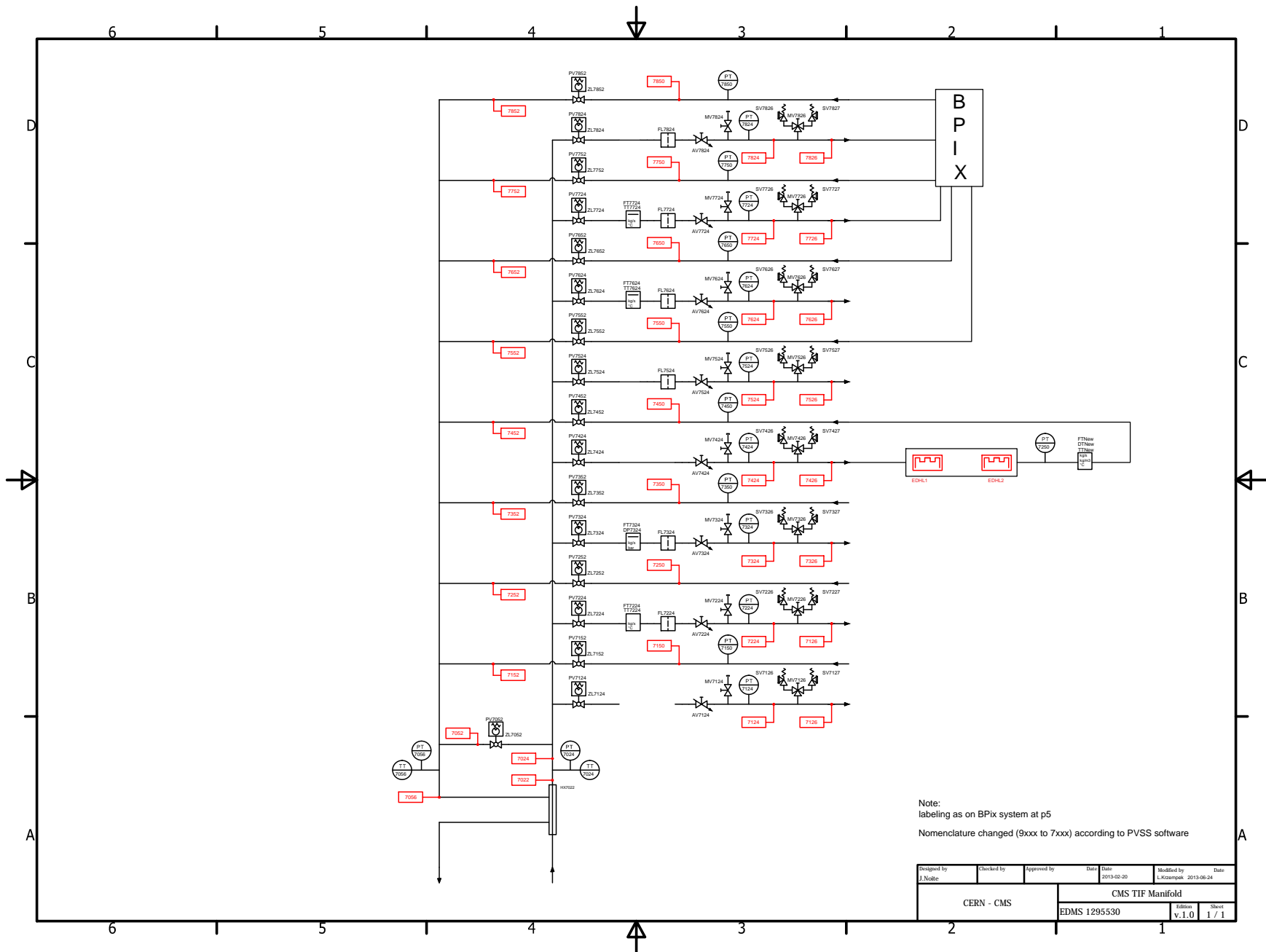
- [1] Tom O'Banion, "Coriolis: the direct approach to mass flow measurement." *Chemical Engineering Progress* 109.3 2013, pp. 41-46.
- [2] REFPROP. NIST REfrigerant Propertiex Database 23, Gaithersburg, MD, 1998, Version 6.01.
- [3] J. Wu et al. "Investigation of heat transfer and pressure drop of CO₂ two-phase flow in a horizontal minichannel." *International Journal of Heat and Mass Transfer* 54.9 2011. pp. 2154-2162.
- [4] R. Mastrullo, A.W. Mauro, A. Rosato, G.P. Vanoli. "Carbon dioxide heat transfer coefficients and pressure drops during flow boiling: Assessment of predictive methods." *International Journal of Refrigeration* 2010, vol. 33, pp. 1068-1085
- [5] R. Mastrullo et al. "Comparison of R744 and R134a heat transfer coefficients during flow boiling in a horizontal circular smooth tube." *International Conference on Renewable Energies and Power Quality (ICREPQ09)*, Valencia, Spain, April 15-17. 2009.
- [6] Yun et al. "Flow boiling heat transfer of carbon dioxide in horizontal mini tubes." *International Journal of Heat and Fluid Flow* 26.5 2005. pp. 801-809.
- [7] International Organization for Standardization. "ISO 10790:2015(E) Measurement of fluid in closed conduits - Guidance to the selection, installation and use of Coriolis flowmeters (mass flow, density and volume flow measurements)." 2015
- [8] R. R. Mastrullo, A.W. Mauro, A. Rosato, G.P. Vanoli. "Carbon dioxide local heat transfer coefficients during flow boiling in a horizontal circular smooth tube." *International Journal of Heat and Mass Transfer* 2009, vol. 52, pp. 4184-4194
- [9] P. Tropea et al. "Design, construction and commissioning of a 15 kW CO₂ evaporative cooling system for particle physics detectors: lessons learnt and perspectives for further development" *Proceedings of Science*, 2014, Paper no. 223

- [10] J. Daguin *et al.* "Evaporative CO₂ Cooling System for the Upgrade of the CMS Pixel Detector at CERN", *10th IIR Gustav Lorentzen Conference on Natural Refrigerants*, 2012, Paper no. 188.
- [11] Krohne Group. "Optimass 6400" Internet: http://optimass6400.krohne.com/#_introduction, [Feb. 18, 2015]
- [12] Krohne Group. "Optimass 6400." Brochure. Apr 2013
- [13] L. Cheng, G. Ribatski, J. M. Quibén, J R. Thome. "New prediction methods for CO₂ evaporation inside tubes: Part I - A two-phase flow pattern map and a flow pattern based phenomenological model for two-phase flow frictional pressure drops." *International Journal of Heat and Mass Transfer* vol. 51, pp. 111-124, 2008
- [14] B. Verlaat. "Controlling a 2-phase CO₂ loop using a 2-phase accumulator." *International Conference of Refrigeration*, 2007, Beijing, China, ICR07-B2-1565
- [15] A.P. Colijn, B. Verlaat. "Evaporative CO₂ Heat Transfer Measurements for Cooling Systems of Partical Physics Detectors." *7th International Conference on Heat Transfer, Fluid Mechanics and Thermodynamics*, 2010, Antalya, Turkey, HEFAT2010
- [16] B. Mishra. "CO₂ based two phase cooling test set up for CMS trackers: Comparison of experiments with theoretical models." *CERN CMS Collaboration*
- [17] B. Verlaat. "CO₂ Cooling Developments for HEP Detectors." *Proceedings of Science*, 2009
- [18] Emerson Electric Co. Video File: "Demonstration: Coriolis Flowmeter excels with Two-Phase Flow (entrained gas)." Retrieved from <https://www.youtube.com/watch?v=AjtdNxDOeoo>, Jan. 17, 2013, [Mar. 15, 2015]
- [19] P. Tropea. "The CMS PIX Phase I upgrade CO₂ cooling: a full scale prototype ready for tests." Internet: <http://ph-news.web.cern.ch/content/cms-pix-phase-i-upgrade-co2-cooling-full-scale-prototype-ready-tests>, Dec. 13, 2013 [Mar. 14, 2015]
- [20] D. Wehrs, A. Klosinski. "Entrained Gas Diagnostic with Intelligent Differential Pressure Transmitter." White Paper: *Emerson Process Management*, Jan. 2008, p. 1
- [21] K. Parker. "Bent-tube Coriolis flowmeter slated for entrained gas, high-temp applications." *Processing Magazine* (Jul. 1, 2013)
- [22] B. Verlaat, "CO₂ cooling is getting hot in high-energy physics." *CERN Courier* (May 31, 2012)

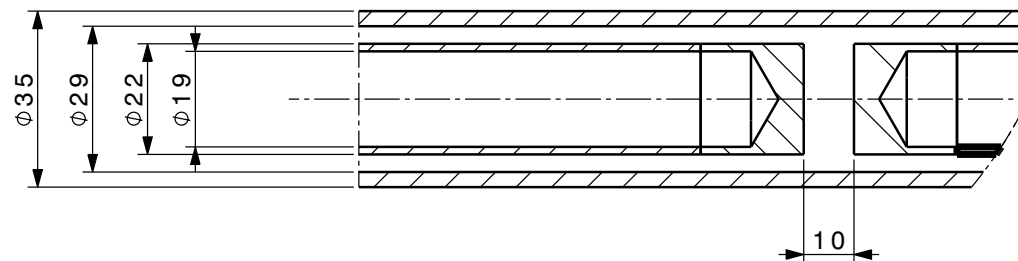
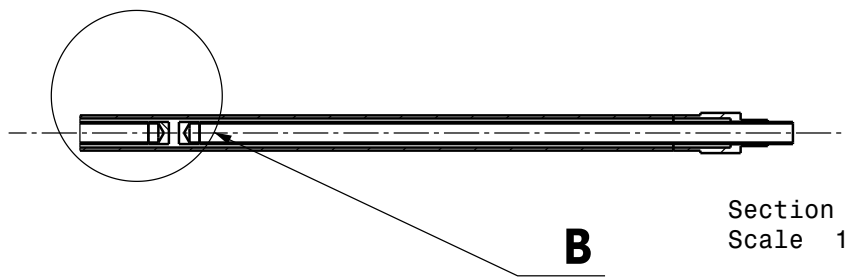
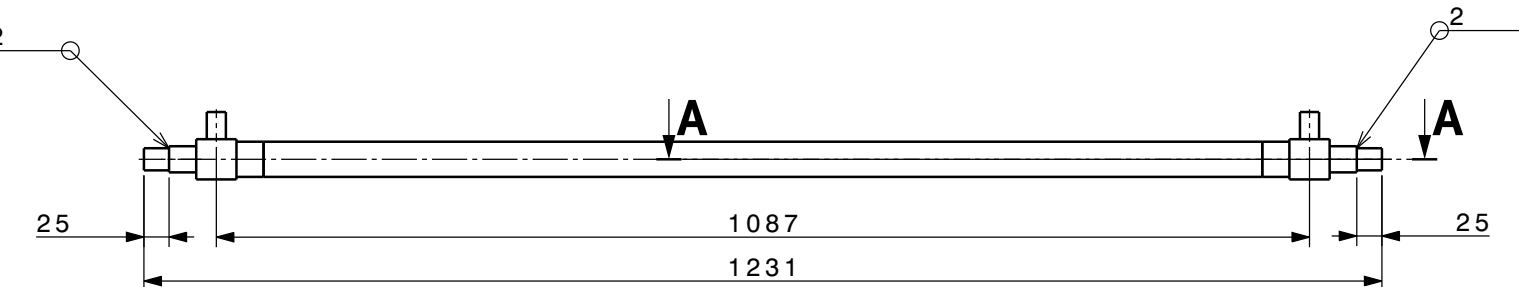
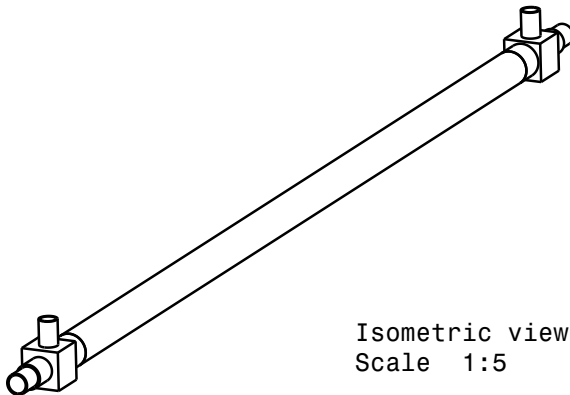
- [23] L. Augyrond *et al.* "Void Fraction Measurement in Two-Phase Helium Flow with Electron Energy Attenuation Detector." *Cryogenic Engineering Conference*, Jul. 2001, Madison, WI, USA C-09B-02
- [24] Jacopo Buongiorno. "NOTES ON TWOPHASE FLOW, BOILING HEAT TRANSFER, AND BOILING CRISES IN PWRs AND BWRs." *MIT OpenCourseWare*. Fall 2010.
- [25] Y. Zhao, Q. Bi, R. Hu. "Recognition and measurement in theflow pattern and void fraction of gas-liquid two-phase flow in vertical upward pipes using the gamma densitometer." *Applied Thermal Engineering* 60 (2013) 398e41
- [26] D. Bauer, H. Chaves, and C. Arcoumanis. "Measurements of void fraction distribution in cavitating pipe flow using x-ray CT." *Measurement Science and Technology*, Issue 23, 2012
- [27] M. Beker. "Capacitive measurement technique for void fraction measurements in two phase pipe flow." BSc Project, Delft University of Science and Technology, Delft, the Netherlands, Jul. 2005
- [28] J. M. Doster, "Flow Regime Mapping, Void-Quality Relations and Pressure Drop in Two Phase Flow." Lecture Notes. Nuclear Engineering Department, North Carolina State University
- [29] B. R. Jean. "A Microwave Sensor for Steam Quality." *IEEE Transaction on Instrumentation and Measurement*, Aug. 2007
- [30] A. Dorfman, E. Fridman. "Vapor quality measurement by a discharging calorimeter." *Fluid Phase Equilibria*, 244 (2006) 4651
- [31] Emerson Process Management. "Explaining how two-phase flow affects mass flowmeters." *Micro Motion, Inc.* 2004

A. The TIF Cooling System



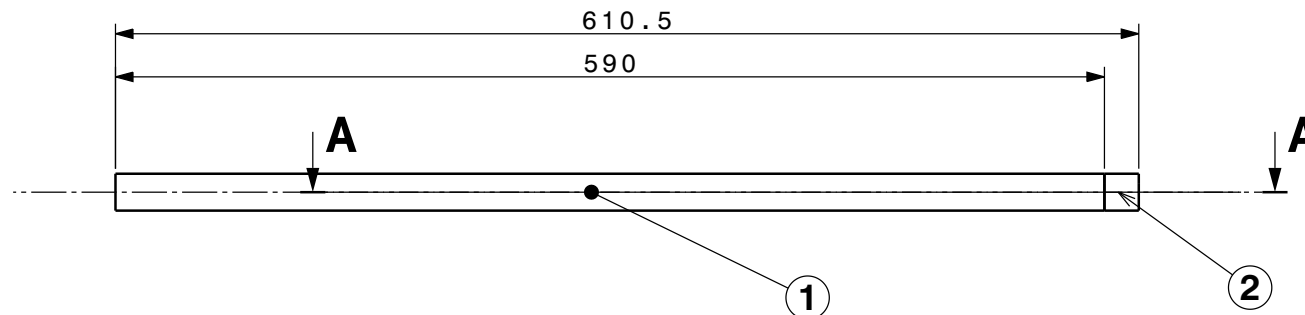


B. Dummy Load Heater Module Mechanical Design

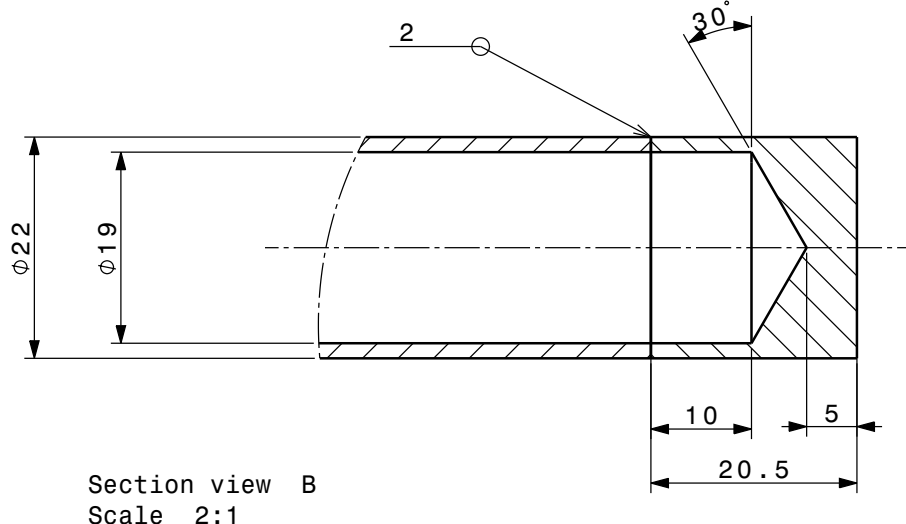


QUANT.	DESCRIPTION	POS.	MAT.	OBSERVATIONS		REF.CERN	
				ENS/ASS	S.ENS/S.ASS		
2	Heatre pipe	3					
1	C02 pipe	2					
2	TEE	1					
NEW HEATER DESIGN				SCALE	DES/DRA.	T. KATOPODIS 2013-09-25	
					CONTROLLED		
					RELEASED		
					APPROVED		
				\ \			
				REMPPLACE/REPLACES			
CERN				NON VALABLE POUR EXECUTION NOT VALID FOR EXECUTION		SIZE IND. 3	
				QAC -		1	
				3		2	

Front view
Scale 1:3

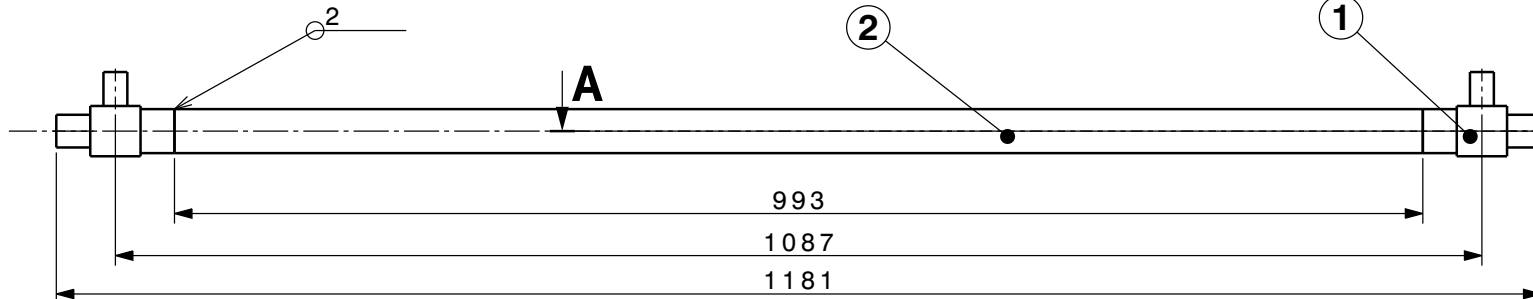


Section view A-A
Scale 1:3

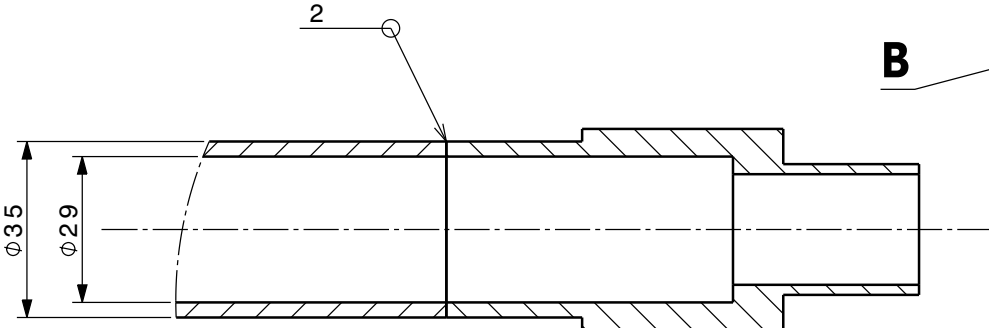


Section view B
Scale 2:1

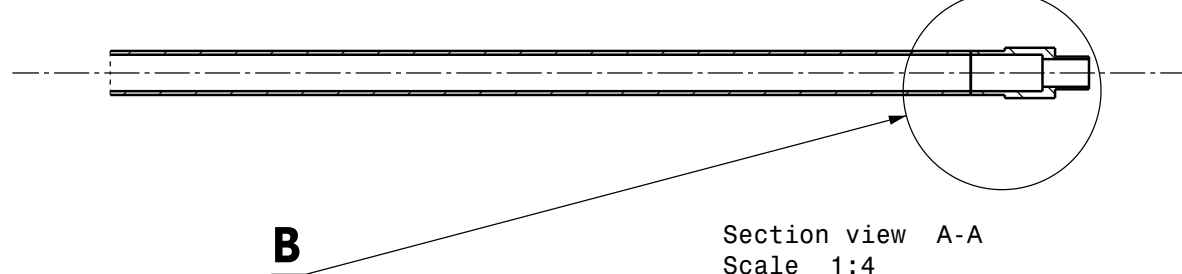
QUANT.	DESCRIPTION	POS.	MAT.	OBSERVATIONS		REF.CERN
				ENS/ASS	S.ENS/S.ASS	
HEATER PIPE						
				ECHELLE	DES/DRA.	T. KATOPODIS 2013-09-25
				SCALE	CONTROLLED	
					RELEASED	
					APPROVED	
					\ \	
					REMPLECE/REPLACES	
CERN	NON VALIDABLE POUR EXÉCUTION NOT VALID FOR EXECUTION			QAC		
	-				SIZE IND. 3	



Front view
Scale 1:4



Section view B
Scale 1:1



Section view A-A
Scale 1:4

1	CO2 pipe	2						
2	TEE	1						
QUANT.	DESCRIPTION	POS	MAT.	OBSERVATIONS			REF.CERN	
	ENS/ASS			S.ENS/S. ASS				
CO2 PIPE WELDED ON TEE				ECHELLE SCALE	DES/DRA.	T. KATOPODIS	2013-09-25	
					CONTROLLED			
					RELEASED			
					APPROVED			
					\\			
					REPLACE/REPLACES			
	NON VALABLE POUR EXECUTION NOT VALID FOR EXECUTION		QAC				SIZE	IND.
			-				3	

C. MATLAB Code

D. Test Log

E. Raw Data